Chem Soc Rev

REVIEW ARTICLE

Cite this: *Chem. Soc. Rev.*, 2018, **47**, 1022

The Bethe–Salpeter equation in chemistry: relations with TD-DFT, applications and challenges

Xavier Blase *[a] Ivan Duchemin[b] and Denis Jacquemin *[c]

Received 24th January 2017

DOI: 10.1039/c7cs00049a

rsc.li/chem-soc-rev

We review the many-body Green's function Bethe–Salpeter equation (BSE) formalism that is rapidly gaining importance for the study of the optical properties of molecular organic systems. We emphasize in particular its similarities and differences with time-dependent density functional theory (TD-DFT), both methods sharing the same formal $\mathcal{O}(N^4)$ computing time scaling with system size. By comparison with higher level wavefunction based methods and experimental results, the advantages of BSE over TD-DFT are presented, including an accurate description of charge-transfer states and an improved accuracy for the challenging cyanine dyes. We further discuss the models that have been developed for including environmental effects. Finally, we summarize the challenges to be faced so that BSE reaches the same popularity as TD-DFT.

1 Introduction

The importance of processes related to electronically excited states (ES) in chemistry, physics and applied technology will continue to rapidly grow in the next few decades. When originating from the interaction between matter and an external electromagnetic field, these phenomena are typically initiated by the absorption of incoming visible light. The applications of photoactive molecules are countless, *e.g.*, in textiles, fluorescence probes, phosphors, solar cells, artificial photosynthesis, photochromes, *etc.* However, in sharp contrast to their ground-state (GS) counterparts, ES are short-lived, making their experimental characterization a costly challenge. For instance, whilst one can find X-ray diffraction data for a plethora of diverse molecular GS structures, accurate ES geometries have been experimentally determined for only a very limited number of small molecules. This is one of the reasons why theoretical methods

[a] *Univ. Grenoble Alpes, CNRS, Inst NEEL, F-38042 Grenoble, France. E-mail: xavier.blase@neel.cnrs.fr*
[b] *Univ. Grenoble Alpes, CEA, INAC-MEM, L-Sim, F-38000 Grenoble, France. E-mail: ivan.duchemin@cea.fr*
[c] *CEISAM UMR CNRS 6230, Université de Nantes, 2 rue de la Houssinière, BP 92208, 44322 Nantes Cedex 3, France. E-mail: Denis.Jacquemin@univ-nantes.fr*

Xavier Blase

Xavier Blase holds his PhD in Physics from the University of California at Berkeley. He is presently CNRS Research Director at Institut Néel, Grenoble, France. His research focuses on the electronic and optical properties of systems relevant to condensed matter physics, materials sciences and physical chemistry, with much emphasis on methodology. He is the co-author of the FIESTA code (Bull-Fourier prize 2014) that implements the GW and Bethe-Salpeter formalisms with Gaussian basis sets. He received the 2008 CNRS silver medal.

Ivan Duchemin

Ivan Duchemin holds his PhD from the CEMES in Toulouse, France. He stayed as a postdoctoral fellow at the UC Davis Physics department, California, and the Max Plank Institute for Polymer Research in Mainz, Germany, before joining the French Center for Alternative Energies (CEA), Grenoble, France, as a senior scientist. His research interests focus on methodological and code developments in ab initio quantum simulations. He is presently the main developer of the FIESTA code (Bull-Fourier prize 2014).

able to deliver ES properties at reasonable computational costs have been in the limelight in the last decade.

One can roughly split the available *ab initio* methods for ES into two main categories: multi-reference and single-reference. The former, *e.g.*, the complete active space with second-order perturbation (CASPT2) method, have the clear advantage of being able to intrinsically treat the crossing between electronic states, notably conical intersections, and can thus deliver high-quality simulations of photochemical processes. Nevertheless, despite recent developments in the field,[1,2] these multi-reference methods remain limited to model chromophores, often far from the extended and highly conjugated dyes of experimental interest. An additional drawback of these multi-reference approaches is that most cannot be used in a black-box manner, meaning that significant manpower is necessary to tackle a specific problem.

The single-reference methods cannot, in their traditional forms, provide crossing points between electronic states, but are easier to apply and allow for systematic and automated applications. In this second group, today's main workhorse is time-dependent density functional theory (TD-DFT),[3–5] that has been used for thousands of applications. The success of TD-DFT can be linked to several advantageous features: (i) a formal $\mathcal{O}(N^4)$ scaling with system size;[3,4] (ii) the coupling with a rather extended panel of environmental models for treating both solvent and solid-state effects;[6–11] (iii) the possibility of including relativistic spin–orbit effects in a computationally efficient way;[12] and (iv) the availability of analytic first and second geometrical derivatives,[13–16] enabling fast exploration of the ES potential energy surfaces and hence the determination of absorption and emission band shapes.[17] However, in its most widely applied form, that is under the so-called adiabatic approximation,[3,18] TD-DFT presents several weak points. First, the results are strongly dependent on the selected exchange–correlation functional (XCF), the impact being particularly strong for charge-transfer (CT) and Rydberg ES.[19] Second, TD-DFT cannot model ES presenting a significant double excitation character, and also produces inaccurate results for cyanine derivatives.[20] This problem can be overcome with the use of double-hybrids,[21,22] but this implies introducing an additional term in the calculation which is detrimental for the computational efficiency. Third, TD-DFT has difficulties in accurately describing singlet–triplet transition energies, a problem that has been thoroughly investigated in the literature.[23–25] Fourth, TD-DFT might deliver incorrect ES ordering when states of different natures (local, CT, *etc.*) have to be described simultaneously, and this holds even in simple molecules, *e.g.*, thiophene.[26] To circumvent these problems, chemists often turn towards single-reference wavefunction-based approaches, and, more precisely to the coupled-cluster (CC)[27–30] and algebraic diagrammatic construction (ADC)[31–33] techniques. These methods generally provide more accurate estimates than TD-DFT and have the additional advantage to allow estimations free of any XCF-dependency that can be systematically improved by increasing the expansion order, *e.g.*, by using CC2, CCSD, CC3, CCSDT, *etc.* However, their computational costs are (much) higher than that of TD-DFT. Indeed, the two simplest second-order approaches, namely ADC(2) and CC2, present a formal $\mathcal{O}(N^5)$ scaling with system size, and, although much efforts have been made in the field,[34,35] the modelling of large systems, easily accessible with TD-DFT, remains beyond reach with these wavefunction theories.

In parallel with the development of the above-mentioned ES methods, other communities developed alternative approaches reflecting their own problematics and systems of interest. Of specific importance for the present review, the so-called many-body Green's function *GW* formalism, where *G* and *W* stand for the time-ordered one-body Green's function and screened Coulomb potential, respectively, was initially designed by Lars Hedin in 1965,[36] the same year as the seminal DFT paper by Kohn and Sham (KS).[37] Using the functional derivative techniques introduced by Martin and Schwinger in 1959,[38] Hedin explored the electronic properties of an interacting homogeneous electron gas, a paradigmatic system in solid-state physics. The *GW* formalism,[36,39–42] aiming at calculating electron addition and removal energies, as obtained by photo-emission experiments (Fig. 1), was first applied at the *ab initio* level in the 1980s to describe the band structure of bulk silicon, diamond and other semiconductors,[43–46] in an attempt to overcome the known deficiency of the DFT Kohn–Sham approach that significantly underestimates band gaps when (semi)local XCF are selected. Applications to more complex bulk systems (see compiled data in ref. 47), including semiconductors erroneously predicted to be metallic by DFT, surfaces, nanotubes, nanowires, and more recently 2D materials, followed with improving computer power and algorithms (for comprehensive reviews, see, *e.g.*, ref. 39, 40 and 48). The *GW* formalism can be considered now as the "gold standard" for band structure calculations in solid-state physics,[49] with an $\mathcal{O}(N^4)$ scaling with respect to system size in its usual planewave implementation. Its ability to describe with good accuracy and without any adjustable or tuned parameters both finite size and extended systems, metallic and insulating materials, certainly contributed to the

Denis Jacquemin

Denis Jacquemin received his PhD in Chemistry from the University of Namur in 1998, before moving to the University of Florida for his postdoctoral stay. He is currently full Professor at the University of Nantes (France). His research is focused on modeling electronically excited-state processes in organic and inorganic dyes and photochromes using a large panel of ab initio approaches. He has been ERC grantee (2011–2016), member of Institut Universitaire de France (2012–2017) and received the Watoc's Dirac Medal (2014).

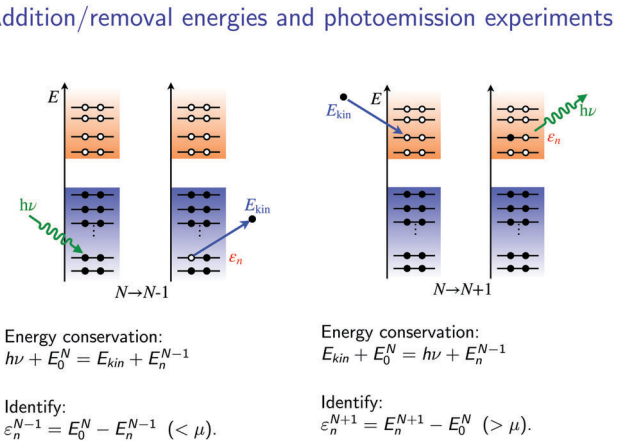

Fig. 1 Sketch of a direct (left) and inverse (right) photoemission experiment used to measure "electronic energy levels" as differences between the $(N-1)$- or $(N+1)$-electron system ground- and excited-states energies and the N-electron system ground-state energy (E_0^N). ε_n^{N-1} and ε_n^{N+1} are the proper occupied and unoccupied energy levels (μ is the chemical potential) that can be used, *e.g.*, to calculate electronic affinities and ionization potentials associated with frontier orbitals. These energies can be obtained as the poles of the Green's function G that lies at the heart of the *GW* and Bethe–Salpeter formalisms.

success of *GW*. In particular, for heterogeneous systems such as organic/inorganic interfaces, including organic molecules deposited on a metallic substrate, for which it may prove difficult to find an optimal XCF suited to both systems in a DFT framework, the *GW* formalism has now become very popular for studying band offsets.[48,50–54]

Parallely, the nuclear physicists Hans Bethe and Edwin Salpeter derived in 1951 the famous Bethe–Salpeter equation (BSE) describing the bound-states of a two-body relativistic system.[55] The BSE approach was later imported in solid-state physics, adopting the screened Coulomb potential W to describe the interaction between the two particles of interest in that field, namely, a photo-excited electron and its related hole, both described at the *GW* level, an approach labeled BSE/*GW* in what follows. This formalism, described in detail in the present Review, generalizes the solid-state-physics textbook's[56] effective-mass approach to extended bulk Mott–Wannier excitons where the long-range electron hole interaction is renormalized by the macroscopic dielectric constant.[57] The first BSE/*GW* applications were devoted to the optical properties of bulk silicon using semi-empirical tight-binding techniques.[58] Pioneering *ab initio* calculations emerged during the 1990s with the exploration of the BSE spectrum of the sodium tetramer,[59] a small hydrogenated silicon cluster,[60] bulk silicon[61] and wide band-gap ionic insulators,[62,63] that is, a variety of systems where electron–hole pairs can be very localized (clusters or ionic systems) or very delocalized (bulk silicon), namely excitons of the (tightly bound) Frenkel or (weakly bound) Mott–Wannier types, respectively.[56] Clear improvements over TD-DFT calculations performed with standard (semi)local functionals were observed for extended systems, with an approach offering the same $\mathcal{O}(N^4)$ computer scaling as TD-DFT.

Table 1 BSE calculations on organic and hybrid systems

Systems	Ref.
Benchmarks singlet ΔE	123–125, 130 and 131
Benchmarks triplet ΔE	124, 128, 129 and 131
Benchmarks osc. str.	126
Polymers (periodic)	64–69
Molecular crystals	70–85
Biological dyes	90–92, 102, 103, 106 and 133–135
Cycloparaphenylene	120
Cyanine dyes	104, 105 and 127
Hybrid materials	94, 115 and 122
Intermolecular CT	94–96, 98, 100, 107, 114, 136 and 137
Intramolecular CT	93, 97, 99, 101, 117, 118, 121, 138 and 139
Fullerenes	88, 98 and 100
Oligoacenes	70–72, 74–76, 78, 83, 84, 87, 111 and 140
Oligothiophenes	82, 97 and 112
Oligomers	80, 82, 97, 101, 112, 120, 136, 137, 141 and 142
Porphyrins	89, 100, 118 and 141
Small molecules	73, 86, 87, 93, 108–111, 113, 119, 123 and 124
Water and ice	113 and 143–146
Bio-inorganic complexes	147–149

Leaving the field of inorganic solid-state physics, pioneering applications of the BSE/*GW* formalism to organic systems appeared as early as 1996 in the case of (periodic) conjugated polymers[64–69] and organic molecular crystals.[70–85] Due to the difficulty in treating gas phase systems with the traditional solid-state physics planewave implementations, calculations on finite molecular systems first tackled small molecules such as methane,[86] benzene and azobenzene,[87] using Gaussian basis sets or real-space grid techniques. Calculations on molecular systems of practical importance, such as fullerenes, porphyrins or chromophores important in dye chemistry, appeared at a rapid pace during the last decade,[82,84,88–120] including large charge-transfer all-organic[95,96,98,100,101,114,121] or hybrid inorganic/organic[94,115,122] structures. We gather in Table 1 some of the available BSE studies on organic systems with indication of the chemical family, and/or the targeted properties, or type of transitions. Despite a decade of intensive applications, it is only much more recently that extensive benchmark assessments of BSE/*GW* appeared.[123–131] These works compare on the same footing, that is, with the same geometries and standard Gaussian basis sets, the results of BSE/*GW* calculations to reference data obtained with wavefunction (CC, ADC or CASPT2) approaches for a large number of optical electronic excitations determined in various organic molecular families. As a signature of its growing use for tackling problematics of the chemistry community (photovoltaics, photochemistry, *etc.*), the BSE/*GW* formalism is starting to appear in standard quantum chemistry packages.[116,132]

In the present Review, we aim to summarize the current state-of-the-art in the BSE/*GW* domain for chemistry applications, which is why we will (i) present the formalism and its connections to the well-known TD-DFT approach; (ii) focus on molecular systems, leaving out "solid-state" applications; and (iii) emphasize both the strengths and weaknesses of the BSE/*GW* theory in a chemical context.

2 Formalism

In the present Review, we do not intend to fully derive the *GW* and Bethe–Salpeter formalisms, using functional derivative techniques or the Feynman diagrammatic language: such derivations can be found in seminal articles, reviews and book chapters listed below. We will rather underline the similarities and differences with the well-known Hartree–Fock (HF), DFT and related time-dependent (TD) TD-HF and TD-DFT formalisms, showing that the concept of self-energy and the related Bethe–Salpeter implementation can be understood as a way of generalizing the standard exchange–correlation potential in DFT as well as the closely related exchange–correlation kernel that enters in the TD-DFT formalism. Such comparisons allow not only to grasp the key ideas behind the *GW* and Bethe–Salpeter methods, but also to provide a potential direction for improving DFT and TD-DFT techniques.

2.1 From the exchange–correlation potential $V^{\mathrm{XC}}[n]$ to the self-energy $\Sigma[G]$

We start with the celebrated DFT KS eigenvalue equation,

$$\left[\hat{h}_0(\mathbf{r}) + V^{\mathrm{H}}(\mathbf{r}) + V^{\mathrm{XC}}[n](\mathbf{r})\right]\phi_n(\mathbf{r}) \overset{\mathrm{DFT}}{=} \varepsilon_n\phi_n(\mathbf{r}), \quad (1)$$

and its Hartree–Fock (HF) analog,

$$\left[\hat{h}_0(\mathbf{r}) + V^{\mathrm{H}}(\mathbf{r})\right]\phi_n(\mathbf{r}) + \int \mathrm{d}\mathbf{r}'\Sigma^{\mathrm{X}}(\mathbf{r},\mathbf{r}')\phi_n(\mathbf{r}') \overset{\mathrm{HF}}{=} \varepsilon_n\phi_n(\mathbf{r}), \quad (2)$$

where $\hat{h}_0$ is the independent-electron Hamiltonian that contains the kinetic energy and the electron–nuclei attraction potential, while V^{XC} is the DFT exchange–correlation potential that contains electronic interactions beyond the classical (Coulombic) Hartree (V^{H}) potential. For reasons apparent below, we introduce the notation Σ^{X} for the exact exchange operator,

$$\Sigma^{\mathrm{X}}(\mathbf{r},\mathbf{r}') = -\gamma(\mathbf{r},\mathbf{r}')v(\mathbf{r},\mathbf{r}') = \frac{-\sum_j^{\mathrm{occ}}\phi_j^*(\mathbf{r})\phi_j(\mathbf{r}')}{|\mathbf{r}-\mathbf{r}'|}, \quad (3)$$

with γ the density matrix and v the bare Coulomb potential. Within DFT, the exchange–correlation potential is a functional of the electron density n, namely: $V^{\mathrm{XC}} = V^{\mathrm{XC}}[n]$, while the true exchange operator is a functional of the density matrix: $\Sigma^{\mathrm{X}} = \Sigma^{\mathrm{X}}[\gamma]$.

The interpretation of the KS or HF eigenvalues as "true" electronic energy levels, that is, as experimentally measurable electron-addition or electron-removal energies in direct or inverse photoemission experiments (see Fig. 1), has been the subject of many articles and reviews (see *e.g.* ref. 150). In short, the KS eigenvalues relying on (semi)local XCF lead generally to rather inaccurate electronic energy levels: the most noticeable drawback is that the HOMO–LUMO gaps in molecular systems, or the band gap in extended semiconductors or insulators, are dramatically underestimated. In contrast, HF leads to too large HOMO–LUMO splitting energies as exemplified in Fig. 2 in the paradigmatic case of pentacene. Such problems paved the way to modern global hybrid (GH) and range-separated hybrid (RSH) XCF with various strategies to tune the admixture of the local exchange–correlation

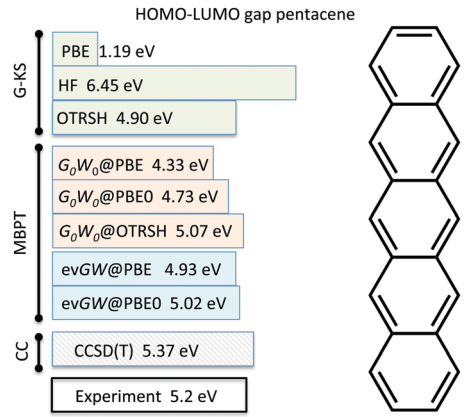

Fig. 2 HOMO–LUMO gap of pentacene as calculated within the Kohn–Sham approach with PBE, or optimally tuned range-separated hybrid (OTRSH) functionals, the Hartree–Fock approach, and with the *GW* approximation to many-body perturbation theory. These values are compared to the difference between the ionization potential (IP) and electronic affinity (AE) as calculated within CCSD(T) or with experimental photoemission. The *GW* data compare non-self-consistent G_0W_0 and partially self-consistent (ev*GW*) calculations starting from PBE or PBE0 Kohn–Sham eigenstates. OTRSH, *GW* and CCSD(T) values are from ref. 140 and were obtained with CBS extrapolation. PBE and HF values were obtained with the same B3LYP geometry and at the aug-cc-pVTZ basis level.

$V^{\mathrm{XC}}[n]$ potential and the non-local exact-exchange $\Sigma^{\mathrm{X}}[\gamma]$ contribution[151–156] in order to obtain accurate electronic energy levels. This is exemplified in Fig. 2 with an "optimally tuned" RSH (OT-RSH, see, *e.g.*, ref. 83, 150 and 157–159), in which the XCF parameters are adjusted so that the KS eigenvalues come close to electron-addition and electron-removal energies.

We now introduce, *in lieu* of the electron density, n, or density-matrix, γ, the time-ordered one-body Green's function $G(\mathbf{r}t,\mathbf{r}'t')$, which is central in the *GW* theory. Leaving exact demonstrations to reference books dedicated to Green's function theory,[41,160] or more specifically to the *GW* formalism,[41,42] the formal definition of $G(\mathbf{r},\mathbf{r}';\omega)$ in its energy representation reads,

$$G(\mathbf{r},\mathbf{r}';\omega) = \sum_i \frac{g_i(\mathbf{r})g_i^*(\mathbf{r}')}{\omega-\varepsilon_i-i\eta} + \sum_a \frac{g_a(\mathbf{r})g_a^*(\mathbf{r}')}{\omega-\varepsilon_a+i\eta}, \quad (4)$$

where η is a positive infinitesimal. The $\{\varepsilon_i, \varepsilon_a\}$ are the "true" charged excitation energies as defined experimentally in direct and inverse photoemission spectroscopy (see Fig. 1). More precisely, we define $\varepsilon_a = E(N+1,a) - E(N,0)$ for unoccupied state energy levels and $\varepsilon_i = E(N,0) - E(N-1,0)$ for occupied energy levels, where $E(N+1,a)$ is the total energy of the $(N+1)$-electron system in its ath quantum state, $E(N-1,i)$ is the total energy of the $(N-1)$-electron system in its ith quantum state, and $E(N,0)$ is the N-electron system GS energy. The $\{g_{i/a}(\mathbf{r})\}$ are called "Lehman amplitudes" and represent the wavefunction overlap between the N-electron GS with one removed/added electron in $(\mathbf{r})$ and the ith/ath excited states of the $(N-1)/(N+1)$ electron systems, respectively. Since G considers processes where one electron is added or removed to the system, it is named a one-particle Green's function, a wording that should not hide that G contains all many-body effects, including in

particular all interactions between the added particle and the N-electrons in the system.

A central and important result is that the Green's function G, for the true interacting system, can be formally shown to be the solution of the following "Dyson" equation,

$$G(1,2) = G^0(1,2) + \int \mathrm{d}34 G^0(1,3)\Sigma^{\mathrm{HXC}}(3,4)G(4,2), \qquad (5)$$

with, *e.g.*, 1 = ($\mathbf{r}_1$,t_1) a space–time coordinate. G^0 is the independent electron Green's function obtained by replacing the $\{\varepsilon_n, g_n\}$ in the definition of G by the independent-electron eigenstates $\{\varepsilon_n^0, \phi_n^0\}$, namely the eigenstates of the one-electron $\hat{h}_0$ operator. The Σ^{HXC} operator contains all the electron–electron interactions (Hartree, exchange and correlation) and is labeled the self-energy operator. This equation indicates that all electron–electron interactions needed to obtain G can be folded into Σ^{HXC} which is a 2-body operator, as the exact exchange Σ^{X} operator in HF theory, except that Σ^{HXC} is dynamical, that is, energy-dependent. The analysis of eqn (5) also shows that the self-energy Σ is a functional of the Green's function G, that is, $\Sigma^{\mathrm{HXC}} = \Sigma^{\mathrm{HXC}}[G]$, rather than a functional of the electron density or of the density-matrix, as in DFT and HF, respectively. The relationships between the HF, DFT and *GW* quantities are summarized in Table 2.

By plugging the definition of G into the time Fourier-transform of the Dyson equation, one obtains an eigenvalue equation,

$$\left[\hat{h}_0(\mathbf{r}) + V^{\mathrm{H}}(\mathbf{r})\right]\phi_n(\mathbf{r}) + \int \mathrm{d}\mathbf{r}' \Sigma^{\mathrm{XC}}(\mathbf{r},\mathbf{r}';\varepsilon_n)\phi_n(\mathbf{r}') = \varepsilon_n\phi_n(\mathbf{r}), \quad (6)$$

where we have renamed the $\{g_n\}$ as $\{\phi_n\}$ and isolated the exchange–correlation self-energy Σ^{XC} from the classical Hartree contribution. In this way, one recovers a "standard" eigenvalue equation in which the $\{\varepsilon_n\}$ energies are the true occupied/empty energy levels as measured in photoemission. What this self-energy formalism tells us is that the exact mapping of the many-body problem into a one-body eigenvalue equation leads to the definition of an exchange–correlation potential $\Sigma^{\mathrm{XC}}(\mathbf{r},\mathbf{r}';\varepsilon_n)$ that should be non-local, as the exact exchange $\Sigma^{\mathrm{X}}(\mathbf{r},\mathbf{r}')$ in the HF theory, but also orbital-energy-dependent, namely it depends on the energy (ε_n) of the state ϕ_n it is acting on.

These results are rather formal and one of the practical questions is to know how the self-energy $\Sigma[G]$ can be written as a function of the Green's function G. This is equivalent to wondering, within the DFT framework, how to write the relationship between the XC potential, $V^{\mathrm{XC}}[n](\mathbf{r})$, and the electron-density, $n(\mathbf{r})$, that is, to define a XCF. While DFT proceeds by exploiting the variational principle, Green's function formalisms usually rely on perturbation theory. In fact, the pioneering developments by the quantum chemistry community attempting to express the self-energy in successive order of the bare Coulomb potential v, yielded, *e.g.*, the ADC(n) methods,[31,32] that are now popular tools for evaluating transition energies.[33] The *GW* approach taken by Hedin in 1964 adopts a different viewpoint by making a connection with the linear response properties of the system, namely by looking at the change of G under a local external perturbation $U(\mathbf{r},t)$. The seminal result, which we will not demonstrate here, is that the functional dependence of Σ^{XC} with respect to G can be explicitly written as:

$$\Sigma^{\mathrm{XC}}(1,2) = -i\int \mathrm{d}345 v(1,3)\left[\frac{\delta G(1,4)}{\delta U(3)}\right]_{U=0} G^{-1}(4,2). \qquad (7)$$

The connection with the response properties of the system allows expressing Σ^{XC} in terms of familiar quantities such as the susceptibility, $\chi(1,2) = \partial n(1)/\partial U(2)$, the inverse dielectric function, ε^{-1}, and the screened Coulomb potential, W:

$$\begin{aligned} W(1,2) &= \int \mathrm{d}3 \varepsilon^{-1}(1,3)v(3,2) \\ &= v(1,2) + \int \mathrm{d}34 v(1,3)\chi(3,4)v(4,2), \end{aligned} \qquad (8)$$

within a set of exact self-consistent equations, the Hedin's equations, leading in particular to:

$$\Sigma^{\mathrm{XC}}(1,2) = i\int \mathrm{d}34 G(1,4)W(3,1^+)\left[\delta(4,3)\delta(2,3) + \frac{\partial \Sigma^{\mathrm{XC}}(4,2)}{\partial V(3)}\right], \qquad (9)$$

with $V = U + V^{\mathrm{H}}$ the sum of the (vanishing) perturbation and the Hartree potential. Since the derivative $(\partial\Sigma^{\mathrm{XC}}/\partial V)$ can further be expressed as a function of W, we obtain to lowest order in the screened Coulomb potential W:

$$\Sigma^{\mathrm{XC}}(\mathbf{r},\mathbf{r}';E) = \frac{i}{2\pi}\int \mathrm{d}\omega \mathrm{e}^{i\omega 0^+} G(\mathbf{r},\mathbf{r}';\omega + E)W(\mathbf{r},\mathbf{r}';\omega), \qquad (10)$$

namely, the well-known *GW* approximation to the exchange–correlation potential Σ^{XC} written in an energy representation. Including higher-order terms leads to the consideration of "vertex corrections" with increased computer cost. For the sake of establishing connections with familiar techniques, the *GW* self-energy can be compared to the expression of the bare exchange in the same Green's function formalism,

$$\Sigma^{\mathrm{X}}(\mathbf{r},\mathbf{r}') = \frac{i}{2\pi}\int \mathrm{d}\omega \mathrm{e}^{i\omega 0^+} G^{\mathrm{HF}}(\mathbf{r},\mathbf{r}';\omega)v(\mathbf{r},\mathbf{r}'), \qquad (11)$$

where G^{HF} is the Hartree–Fock Green's function obtained from eqn (4) by setting $\{g_n, \varepsilon_n\}$ to the HF eigenstates and eigenvalues. As such, the *GW* formalism can be loosely defined as a dynamically screened exchange formalism.

Table 2 Corresponding quantities and their relation within DFT, HF and one-body Green's function (G) formalisms. The time ($t^+ = t + 0^+$) is infinitesimally larger than (t)

Density	Density matrix	1-Body G
$n(\mathbf{r}t) = -iG(\mathbf{r}t,\mathbf{r}t^+)$	$\gamma(\mathbf{r},\mathbf{r}',t) = -iG(\mathbf{r}t,\mathbf{r}'t^+)$	$G(\mathbf{r}t,\mathbf{r}'t')$
Exchange correlation potential	"Bare" exchange HF and hybrids	Self-energy (*GW*)
$V^{\mathrm{XC}}[n](\mathbf{r})$	$\Sigma^{\mathrm{X}}[\gamma](\mathbf{r},\mathbf{r}')$	$\Sigma^{\mathrm{XC}}[G](\mathbf{r},\mathbf{r}';E)$

2.2 Practical *GW* theory: from G_0W_0 to self-consistent approaches

In practice, the input Green's function G needed to build Σ^{XC} is constructed from the "best available" one-body eigenstates, that is typically KS eigenstates that are plugged into eqn (4) to obtain G, whereas the susceptibility, χ, is built from the corresponding KS independent-electron susceptibility χ_0:

$$\chi_0(\mathbf{r},\mathbf{r}';\omega) = \sum_{m,n}(f_m - f_n)\frac{\phi_m^*(\mathbf{r})\phi_n(\mathbf{r})\phi_n^*(\mathbf{r}')\phi_m(\mathbf{r}')}{\omega - (\varepsilon_m - \varepsilon_n) + i0^+}, \quad (12)$$

within, generally, a time-dependent Hartree scheme: $\chi = \chi_0 + \chi_0 v\chi$. The knowledge of G and $\chi(\omega)$, leading to $W(\omega)$, allows obtaining the self-energy Σ^{XC} in the *GW* approximation (GWA). One can then correct the input Kohn–Sham eigenstates by replacing the DFT exchange–correlation potential (V^{XC}) contribution by its self-energy Σ^{XC} analog, namely, by using:

$$\varepsilon_n^{GW} = \varepsilon_n^{KS} + \langle\phi_n^{KS}|\Sigma^{XC}(\varepsilon_n^{GW}) - V^{XC}|\phi_n^{KS}\rangle, \quad (13)$$

where, as can be seen, Σ^{XC} needs to be calculated at the targeted ε_n^{GW} energy. When starting from KS eigenstates generated with a specific XCF, *e.g.*, with the PBE0 global hybrid,[153] one labels this theoretical protocol as G_0W_0@PBE0 to describe the used approach. In this notation, the "0" indexes for G and W indicate that, in the spirit of perturbation theory, the perturbation ($\Sigma^{XC} - V^{XC}$) is built from the input (0th-order) Kohn–Sham eigenstates. Such an approach, even though dramatically improving the KS result in the case of semilocal XCF, is characterized by a rather large "starting point" dependency. Indeed, the G_0W_0 electronic energy levels can significantly vary with the choice of different XCF for the starting KS-DFT calculations (see Fig. 2 and below). Strategies based on the use of input Kohn–Sham eigenstates generated with tuned global or range-separated hybrids, yielding already reliable electronic energy spectra at the Kohn–Sham level, offer a promising direction to reach accurate electronic energy levels from such "single-shot" G_0W_0 calculations as shown in Fig. 2 with the G_0W_0@OTRSH results.[83,161–163]

Alternatively, one can use the corrected eigenvalues to recalculate G, χ_0, W and Σ, a partially self-consistent scheme labelled ev*GW*. In this approach, the input KS eigenvectors, that is, the molecular orbital coefficients, are conserved (frozen), whereas the KS eigenvalues are updated. Such a method allows improving the quality of the *GW* electronic energy levels, removing much of the starting point dependency, as we discuss below. Self-consistent schemes beyond the simple update of the eigenvalues can be performed but at a significantly higher computational cost. The quasiparticle self-consistent *GW* (QS*GW*) approach proceeds by diagonalizing a symmetrized self-energy operator in the starting Kohn–Sham basis in order to update both eigenstates and eigenvalues,[164] while fully self-consistent approaches (SC*GW*) have also been used since the early days of the GW technique.[36] Finally, intermediate techniques with update of only the Green's function (GW_0) have been explored[140] with the advantage that the screened Coulomb potential W does not need to be recalculated. Benchmark *GW* calculations exploiting reference CCSD(T) calculations on extended atomic or molecular sets appeared recently,[83,163,165–168] indicating that the improvements brought by the fully (SC*GW*) or quasiparticle (QS*GW*) self-consistent calculations are somehow disappointing with respect to their associated computational cost. This leaves simple G_0W_0 techniques with optimal Kohn–Sham starting point and partially self-consistent ev*GW* calculations as accurate and useful practical schemes allowing the study of systems comprising more than one hundred atoms[54,96,100,101] thanks to the $\mathcal{O}(N^4)$ formal scaling in standard *GW* implementations. As a final note, we stress that, similarly to the techniques used to fasten ADC(2) and CC2, *e.g.*, Laplace transforms,[35,169] the scaling of *GW* calculations can be further reduced by using appropriate algorithms that have been appearing recently,[170–172] paving the way to applications on even larger systems.

2.3 From TD-DFT to Bethe–Salpeter

We can now proceed from TD-DFT to the Bethe–Salpeter equation (BSE) by "replacing" the electron density $n(\mathbf{r})$ with the Green's function G as the central variable, and the exchange–correlation potential $V^{XC}[n]$ by the generalized self-energy $\Sigma^{XC}[G]$. Rather naturally, while the TD-DFT formalism introduces the susceptibility $\chi(1,2)$ as the linear response coefficient between the variations of the electron density n with respect to a local external perturbation U,[3,4] the BSE approach considers a generalized "4-point" response coefficient $L(1,2;3,4)$ as the variation of the Green's function G with respect to a non-local perturbation U,

$$\chi(1,2) \overset{\text{TD-DFT}}{=} \frac{\partial n(1)}{\partial U(2)} \Rightarrow L(1,2;3,4) \overset{\text{BSE}}{=} -i\frac{\partial G(1,2)}{\partial U(3,4)}, \quad (14)$$

with the relation: $\chi(1,2) = L(1,1;2,2)$ since $n(1) = -iG(1,1^+)$ (see Table 2). Similarly, the standard TD-DFT formula relating χ to the independent-electron susceptibility χ_0 through,

$$\chi(1,2) = \chi_0(1,2) + \int \mathrm{d}34\ \chi_0(1,3)K^{DFT}(1,2)\chi(4,2), \quad (15)$$

where the DFT kernel, K is defined as:

$$K^{DFT}(1,2) = v(1,2) + \frac{\partial V^{XC}(1)}{\partial n(2)}, \quad (16)$$

is replaced in BSE by:

$$L(1,2;3,4) = L^0(1,2;3,4) + \int \mathrm{d}5678 L_0(1,2;3,4)\Xi^{BSE}(5,6,7,8)L(7,8;3,4), \quad (17)$$

that stems from deriving the Dyson equation, eqn (5), by $U(3,4)$, with $L^0(1,2;3,4) = \partial G_0(1,2)/\partial U(3,4)$, the independent-particle 4-point response, and Ξ^{BSE}, a generalized kernel that derives from the exchange–correlation self-energy,

$$\Xi^{BSE}(5,6,7,8) = v(5,7)\delta(5,6)\delta(7,8) + \frac{\partial\Sigma^{XC}(5,6)}{\partial G(7,8)} \quad (18)$$

that can be compared to its TD-DFT analogue, eqn (16), the bare Coulomb potential term (v) originating in both cases from the derivation of the Hartree potential. Plugging now the *GW* approximation for the exchange–correlation self-energy, one obtains,

$$\Xi^{\mathrm{BSE}}(5,6,7,8) = v(5,7)\delta(5,6)\delta(7,8) - W(5,6)\delta(5,7)\delta(6,8) \tag{19}$$

where we have neglected the $(\partial W/\partial G)$ derivative, following the common assumption that the variations of the screening properties with respect to variations of G can be neglected to lowest order. Finally, the common approximation in the BSE community which is the exact equivalent of the static kernel approximation within TD-DFT,[3] that is, the adiabatic approximation, is generally applied. Indeed, one assumes that $W(1,2) \simeq W(\mathbf{r}_1 t_1, \mathbf{r}_2 t_2)\delta(t_1 - t_2)$, *i.e.*, one restricts W to its static limit: $W(\mathbf{r}_1,\mathbf{r}_2;\omega = 0)$. Fig. 3 offers a diagrammatic representation of the BSE theory in terms of propagating holes and electrons, with non-interacting and interacting processes.

Expressing the response functions in their energy representation $L(\mathbf{r}_1\mathbf{r}_2\mathbf{r}_3\mathbf{r}_4;\omega)$ and projecting the space variables onto the molecular orbitals $\{\phi_{i/a}\}$ allow expressing the excitonic Hamiltonian in the usual $\phi_i(\mathbf{r})\phi_a(\mathbf{r}')$ "transition" product basis, and the excitation energies become the solution of the familiar eigenvalue equation:

$$\begin{pmatrix} R & C \\ -C^* & -R^* \end{pmatrix} \cdot \begin{pmatrix} X_\lambda \\ Y_\lambda \end{pmatrix} = \Omega_\lambda \begin{pmatrix} X_\lambda \\ Y_\lambda \end{pmatrix}, \tag{20}$$

with electron–hole eigenstate solutions reading:

$$\psi_\lambda^{\mathrm{BSE}}(\mathbf{r}_\mathrm{e},\mathbf{r}_\mathrm{h}) = \sum_{ia} \left\{ X_\lambda^{ia}\phi_i(\mathbf{r}_\mathrm{h})\phi_a(\mathbf{r}_\mathrm{e}) + Y_\lambda^{ia}\phi_i(\mathbf{r}_\mathrm{e})\phi_a(\mathbf{r}_\mathrm{h}) \right\},$$

where $\{\lambda, i, a\}$ index the optical excitations, and the occupied and unoccupied levels, respectively. In direct similarity with TD-DFT, the X_λ^{ia} are the resonant (occup. → unoccup.) components whereas the Y_λ^{ia} provide the non-resonant (unoccup. → occup. deexcitation) contributions. Neglecting the non-resonant contributions leads, as in TD-DFT, to the Tamm–Dancoff approximation (TDA). Focusing on singlet excitations, the "resonant" Hamiltonian block reads:

$$\begin{aligned} R_{ai,bj}^{\mathrm{BSE}} &= \delta_{a,b}\delta_{i,j}\left(\varepsilon_a^{GW} - \varepsilon_i^{GW}\right) \\ &\quad - \left\langle \phi_a(\mathbf{r})\phi_i(\mathbf{r}')W(\mathbf{r},\mathbf{r}')\phi_b(\mathbf{r})\phi_j(\mathbf{r}') \right\rangle \\ &\quad + 2\left\langle \phi_a(\mathbf{r})\phi_i(\mathbf{r})v(\mathbf{r},\mathbf{r}')\phi_b(\mathbf{r}')\phi_j(\mathbf{r}') \right\rangle \end{aligned} \tag{21}$$

that can be compared to its time-dependent Hartree–Fock,

$$\begin{aligned} R_{ai,bj}^{\mathrm{TD\text{-}HF}} &= \delta_{a,b}\delta_{i,j}\left(\varepsilon_a^{\mathrm{HF}} - \varepsilon_i^{\mathrm{HF}}\right) \\ &\quad - \left\langle \phi_a(\mathbf{r})\phi_i(\mathbf{r}')v(\mathbf{r},\mathbf{r}')\phi_b(\mathbf{r})\phi_j(\mathbf{r}') \right\rangle \\ &\quad + 2\left\langle \phi_a(\mathbf{r})\phi_i(\mathbf{r})v(\mathbf{r},\mathbf{r}')\phi_b(\mathbf{r}')\phi_j(\mathbf{r}') \right\rangle \end{aligned} \tag{22}$$

and TD-DFT counterparts,

$$\begin{aligned} R_{ai,bj}^{\mathrm{TD\text{-}DFT}} &= \delta_{a,b}\delta_{i,j}\left(\varepsilon_a^{\mathrm{KS}} - \varepsilon_i^{\mathrm{KS}}\right) \\ &\quad - \left\langle \phi_a(\mathbf{r})\phi_i(\mathbf{r}')v_\mu^{\mathrm{LR}}(\mathbf{r},\mathbf{r}')\phi_b(\mathbf{r})\phi_j(\mathbf{r}') \right\rangle \\ &\quad + 2\left\langle \phi_a(\mathbf{r})\phi_i(\mathbf{r})K^{\mathrm{DFT}}(\mathbf{r},\mathbf{r}')\phi_b(\mathbf{r}')\phi_j(\mathbf{r}') \right\rangle \end{aligned} \tag{23}$$

where we have selected, for pedagogy, a range-separated hybrid incorporating some long-range v_μ^{LR} exact exchange contribution. As shown by the comparison between the various formalisms, the BSE/*GW* approach starts with the *GW* occupied/unoccupied electronic energy levels, instead of the KS energy levels in the TD-DFT approach. The standard interpretation of the BSE/*GW* scheme is that the *GW* spectrum provides accurate occupied/virtual energy levels, that can be directly compared to experimental electron addition or removal energies, while the BSE scheme adds the $\langle 2v - W \rangle$ matrix elements that represent the electron–hole interaction leading to a reduction of the optical gap as compared to the (photoemission) HOMO–LUMO gap.

Before turning to reviewing recent benchmarks and applications of the BSE theory performed on large molecular sets, let us illustrate the differences between TD-DFT and BSE in the case of the thymine nucleobasis for which highly-accurate reference wavefunction calculations exist, namely CCSD(T) calculations of the ionization potentials and electronic affinities,[173] and CC3 calculations of the S_1 optical excitation energy.[174] Fig. 4 gives the KS HOMO–LUMO gaps and lowest TD-DFT S_1 singlet excitation energies for the compound calculated with the PBE and PBE0 XCF. The DFT/TD-DFT results are compared to the corresponding ev*GW* and BSE data starting from either PBE or PBE0 KS eigenstates. Both TD-DFT and BSE calculations provide a lowest S_1 singlet excitation energy which is in good, even excellent, agreement with the reference CC3 value. However, in the TD-PBE case, the optical absorption (S_1) onset is larger than the KS HOMO–LUMO gap, which is dramatically smaller than the reference values. With PBE0, the KS gap is significantly improved compared to PBE, but remains too small compared to the reference calculations. In contrast, the ev*GW* gap is in close agreement with reference

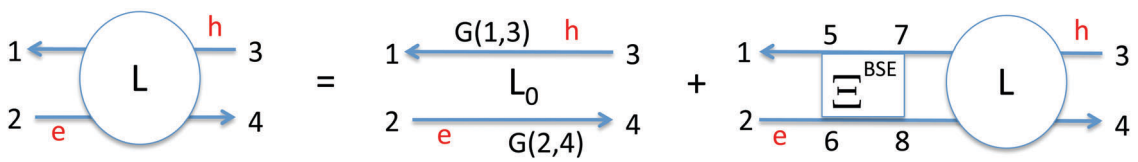

Fig. 3 Diagrammatic representation of the Bethe–Salpeter formalism: $L(1,2;3,4)$ represents the propagation of an electron–hole pair as a coherent superposition of free electron and free hole propagation (L_0) plus processes where electron and hole interact *via* the kernel Ξ^{BSE} that contains the screened Coulomb potential W interaction and a bare exchange term (see eqn (19)).

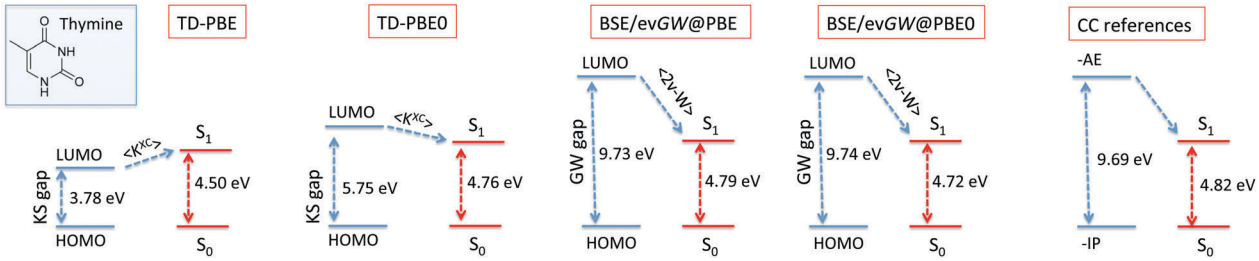

Fig. 4 HOMO–LUMO gap and lowest singlet absorption energy ($1^1A''$) for thymine as calculated within (left) DFT and TD-DFT, with XCF = PBE or PBE0, (center) ev*GW*@XCF and BSE/ev*GW*@XCF with the same XCF, and (right) reference quantum chemistry calculations, namely CCSD(T) for the HOMO–LUMO energies and CC3 for the S_1 energy (from ref. 173 and 174). All calculations performed with the aug-cc-pVTZ atomic basis set (see details in ref. 123).

values using both starting XCF, and the electron–hole interaction, contained in the BSE formalism, stabilizes the electron–hole pair by *ca.* 4.9 eV, the "exciton" binding energy, bringing the BSE transition energy in close agreement with the CC3 reference. The present case of thymine also illustrates the stability of the ev*GW* and BSE/ev*GW* data upon changing the starting XCF.

3 Applications

In this section, we will first describe the results obtained in "general" benchmarks of the BSE/*GW* energies and oscillator strengths, before setting a specific focus on CT, cyanine and triplet excitations, three families of ES that are known to be challenging for standard TD-DFT (see Introduction). Eventually, we discuss a few representative uses of the BSE theory within more applied contexts.

3.1 Benchmarks: transition energies

As emphasized in the Introduction, the applications of the BSE/*GW* formalism for the study of organic systems started to appear in the late 1990s with the study of periodic systems (molecular crystals, polymers, *etc.*) and comparisons were directly made with available experimental optical measurements. More recently, the development of several codes implementing BSE/*GW* with the very same techniques as the one used in quantum chemistry, namely the use of Gaussian bases with explicit calculations of 4-center 2-electron Coulomb integrals, or 3-center approximants using accurate Coulomb-fitting resolution-of-identity (RI) techniques similar to the one often used in TD-DFT, ADC and CC codes, allowed a direct comparison with highly-correlated wavefunction approaches, such as CASPT2 and CC3. Benchmark BSE calculations could then be conducted using the same geometries and basis sets as in the "traditional" quantum chemistry calculations. This allowed extensive comparisons to be carried out for several families of molecular systems (quinones, porphyrins, cyanines, *etc.*) and optical excitations (π–π*, n–π*, CT, Rydberg, singlets and triplets, *etc.*)[123–130] so that the "expected" accuracy of BSE/*GW* can now be estimated for transition energies of molecules.

Since the BSE excitation energies are built upon the *GW* energy levels, the accuracy of the BSE excitation energies is obviously related to that of the preceding *GW* calculation. This was nicely illustrated by Bruneval and co-workers,[124] who correlated the BSE/G_0W_0 error to the corresponding G_0W_0 error on the HOMO–LUMO gap for the well-known Thiel's set of compounds,[174–176] that encompasses 103 singlet and 63 triplet transition energies determined for 28 representative molecules (unsaturated aliphatic hydrocarbons, aromatic compounds, aldehydes, ketones, amides and nucleobases). For this set, theoretical best estimates (TBE) mainly obtained at the CASPT2 or CC3 level for optical transitions,[175] and at the CCSD(T) level for electronic energy levels, are available. Exploiting the fact that non-self-consistent G_0W_0 calculations display a very significant dependence on the starting KS eigenstates, the accuracy of the HOMO–LUMO gap, as compared to CCSD(T), could be controlled by tuning the XCF used to generate the input DFT eigenstates of the G_0W_0 calculations.[124] As shown in Fig. 5, the subsequent error on the BSE singlet excitation energies correlates nicely with the error on the G_0W_0 HOMO–LUMO gap. Further, the BSE average error for singlet excitations comes close to zero when the G_0W_0 error on the gap comes below a very few tenths of an eV.[124] Although the optical excitation energies – even low-lying – are not purely ascribable

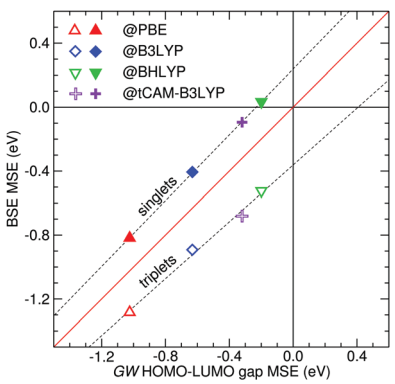

Fig. 5 Correlation between the mean-signed error (MSE) on the BSE/G_0W_0@XCF optical excitation energies and the corresponding MSE for the non-self-consistent G_0W_0@XCF HOMO–LUMO gap where XCF are various global (PBE, B3LYP, BHLYP) or range-separated hybrid (tCAM-B3LYP) XCF. The average is taken over Thiel's set of molecules (see text) and the error is calculated with respect to CCSD(T) values for G_0W_0 data and TBE for BSE excitations. Filled/empty symbols correspond to the lowest singlet/triplet BSE excitations. Reprinted with permission from ref. 124. Copyright 2015 American Institute of Physics.

to the HOMO–LUMO transition, such a correlation illustrates that a prerequisite to an accurate BSE calculation is an accurate *GW* estimate of the orbital energies. This can be reached with several strategies, *i.e.*, one can optimize the starting Kohn–Sham energy levels for a non-self-consistent G_0W_0 approach, or one can use an (affordable) self-consistency approach, such as the ev*GW* scheme. This is what is illustrated in Fig. 4 in the case of thymine where ev*GW* calculations starting from either PBE or PBE0 are found to yield very close and accurate HOMO–LUMO gaps, resulting in accurate and similar BSE S_1 singlet excitation energies. This latter BSE/ev*GW* strategy was applied to the same Thiel's set by us.[123] We showed that BSE/ev*GW* excitation energies determined starting from PBE or PBE0 are within 0.1 eV of each other and show a linear correlation coefficient of 0.99. As compared to the TBE values, the BSE/ev*GW*@PBE0 mean absolute error (MAE) is equal to 0.25 eV for singlet excitations, clearly outperforming the corresponding BSE/G_0W_0@PBE0 perturbative approach that yields a MAE of 0.62 eV.[123] It is important to stress that, for the same set of transitions, that do not encompass charge-transfer nor cyanine excitations, the MAE obtained with TD-PBE0 and CC2 are both 0.23 eV.[123,176] In other words, for that specific set, TD-PBE0 is clearly the most effective approach in terms of accuracy/time ratio. However, the BSE/ev*GW* results have the clear-cut advantage of being much less dependent on the XCF than their TD-DFT counterparts, *e.g.*, the TD-PBE and TD-CAM-B3LYP MAE are 0.53 eV and 0.31 eV, respectively,[177] both significantly larger than the TD-PBE0 error.

The advantage of BSE/ev*GW* in terms of XCF-dependency over "standard" TD-DFT has also been illustrated using the recently proposed Truhlar–Gagliardi set of molecular transitions.[178] This set includes valence (both n–π* and π–π*), Rydberg and CT ES and reference values are taken from both experiment and theory (see ref. 178 for details). As illustrated in the left panel of Fig. 6, doubling the amount of exact exchange included in the XCF by going from M06 (27%) to M06-2X (54%),[156] induces, as expected,[19] a strong increase of the computed TD-DFT transition energies, especially for the triplet, Rydberg, and CT ES. The average increase is +0.34 eV for the 23 considered transitions.[131] In contrast, when going from BSE/ev*GW*@M06 to BSE/ev*GW*@M06-2X (right panel in Fig. 6), the variations of the transition energies induced by the XCF change are clearly strongly reduced, with an average change of +0.09 eV.[131] The only exceptions to this reduction are the n–π* transitions, that undergo similar absolute changes at both TD-DFT and BSE/ev*GW* levels, a specific aspect that has been investigated in a separate contribution.[130] In Table 3, we list the MAE obtained for several methods, using as reference, the values given by Truhlar and Gagliardi.[178] As can be seen, for this specific set, BSE/ev*GW* outperforms EOM-CCSD and provides an average deviation equivalent to the one obtained with CASPT2, irrespective of the starting XCF, which is certainly a significant success as BSE/ev*GW* is much less computationally demanding than these two wavefunction approaches. The errors obtained with TD-DFT are larger, especially with TD-M06 that delivers poor estimates for both Rydberg and CT transitions. However, one also notices that the linear determination coefficients determined with respect to the reference values obtained with BSE/ev*GW* are significantly smaller than their EOM-CCSD and CASPT2 counterparts, that is, the "consistency" of the BSE/ev*GW* results is rather similar to the one obtained with TD-DFT.

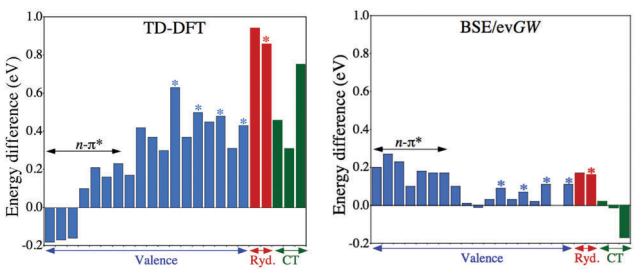

Fig. 6 Impact of the change of XCF (from M06 to M06-2X) on the excitation energies determined with TD-DFT (left) and BSE/ev*GW* (right). The blue, red and green histograms correspond to valence, Rydberg and CT transitions, respectively. The stars indicate singlet–triplet transitions. All values are in eV. Adapted with permission from ref. 131, Copyright 2017, American Chemical Society.

Table 3 MAE (in eV) for different subsets of excitations for the Truhlar–Gagliardi set of compounds (aug-cc-pVTZ atomic basis set). In the rightmost column, we also list the linear determination coefficient, R^2, determined for the whole set of compounds. Values taken from ref. 131 and 178, the total MAE is computed as 1/3 valence + 1/3 Rydberg + 1/3 CT

	MAE				
Method	Valence	Ryd.	CT	Total	R^2
EOM-CCSD	0.27	0.24	0.42	0.31	0.98
CASPT2	0.15	0.20	0.29	0.21	0.99
TD-M06	0.29	0.78	0.57	0.55	0.92
TD-M06-2X	0.22	0.11	0.40	0.25	0.95
BSE/ev*GW*@M06	0.31	0.25	0.09	0.21	0.95
BSE/ev*GW*@M06-2X	0.28	0.12	0.15	0.18	0.95

Besides the above-described "theoretical" benchmarks, comparisons with experimental data have also been made. This however is not as straightforward for at least three reasons: (i) one should select an atomic basis set large enough so as to deliver transition energies close enough to convergence; (ii) the vast majority of experimental measurements are carried out in condensed phases, and the impact of the environment tends to be large for ES properties; and (iii) the vertical approximation, that is, the consideration of a pure Franck–Condon transition neglecting all vibrational effects, does not allow physically-sound comparisons with experiments. In fact, the data affording the most straightforward theory/experiment comparisons are the 0–0 energies,[21,179,180] but, on the theoretical side, they require the determination of vibrational energies of both the GS and the ES, that, to date, have not been obtained from BSE/*GW* calculations due to the lack of analytical derivatives (see Section 5.1). To circumvent these difficulties, while still offering fair comparisons between TD-DFT, BSE/ev*GW* and wavefunction methods, a specific protocol was set up in ref. 125. In this protocol, the geometries and vibrational frequencies are determined with TD-DFT, and more precisely TD-M06-2X, the solvent effects are accounted for

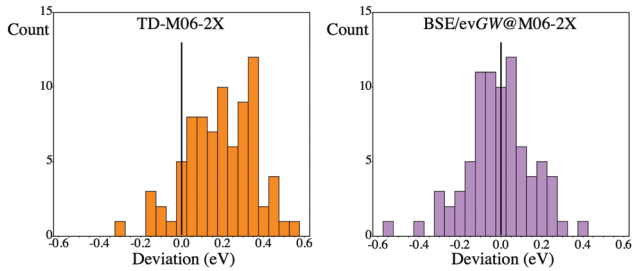

Fig. 7 Histograms showing the repartition of the deviations of the TD-M06-2X (left) and BSE/ev*GW*@M06-2X (right) 0–0 energies compared to their CC2 counterparts for 80 organic dyes. All values are in eV and have been obtained on exactly the same geometries. Adapted with permission from ref. 125, Copyright 2017, American Chemical Society.

using a state-specific continuum model,[7] whereas the vertical transition energies are determined with different methods using a large atomic basis set, namely, aug-cc-pVTZ, that is known to provide converged results at both BSE/ev*GW*[181] and CC2 levels of theory.[182] With this hybrid computational protocol, the 0–0 energies determined with TD-DFT, BSE/ev*GW*, ADC(2) and CC2 could be compared to experimental measurements for 80 fluorescent dyes containing between *ca.* 20 and 70 atoms.[125] In Fig. 7, we report histograms showing the deviations of the TD-DFT and BSE/ev*GW* 0–0 energies taking the CC2 values as reference. It is clear that TD-M06-2X has a tendency to deliver 0–0 energies significantly above the CC2 values. If this effect could be attenuated by selecting a XCF with a smaller ratio of exact exchange, this would probably be at the cost of increasing the dispersion around the reference data.[183] In contrast, the BSE/ev*GW* values are symmetrically spread around the CC2 energies, with only two cases with differences exceeding 0.4 eV.[125] Table 4 provides comparisons with measured 0–0 data, considering various subsets of compounds and methodologies. Obviously, the average errors with respect to experiment are similar with BSE/ev*GW*, ADC(2) and CC2, *ca.* 0.15 eV, and are also rather equivalent for both CT and cyanine derivatives, which constitutes an impressive results. In contrast, TD-M06-2X delivers significantly larger deviations, especially for cyanine derivatives, an aspect that is detailed in Section 3.4.

To close this section, it is worth pointing out that two studies benchmarked BSE/*GW* for small compounds containing transitions metals.[108,119] In the former investigation, the authors explored a set of 39 small inorganic molecules[108] and obtained, with BSE/ev*GW*@PBE0, a MAE of *ca.* 0.3 eV compared to experiment, slightly above the result reached with TD-PBE0 (MAE of *ca.* 0.2 eV). In the latter work, the authors considered transition metal atoms (Cu, Zn, Ag, and, Cd) as well as their monoxide anions,[119] and evaluated numerous BSE/*GW* flavors, including some *GW* approaches with vertex corrections. Using either BSE/ev*GW* or BSE/G_0W_0 with vertex corrections, they obtained a MAE of *ca.* 0.2 eV for their test set. Consequently, these two works hint that the BSE/*GW* mean absolute deviations reported in the above-described benchmarks of organic compounds are not strongly different from the one that can be obtained on compounds containing transition metal atoms.

3.2 Benchmarks: oscillator strengths

Fewer studies have been devoted to the assessment of the accuracy of the BSE/ev*GW* oscillator strength, *f*, though they are also of prime importance for interpreting experimental measurements. In fact, we are aware of only one general benchmark devoted to this topic.[126] In contrast, the TD-DFT *f* values have been the subject of several studies,[184–188] and the same holds for wavefunction approaches.[189–191] A major difficulty in the field is to obtain accurate reference data, *e.g.*, for the above-mentioned Thiel's set, CC3 *f* are significantly smaller than their CC2 counterparts (see also below).[190] This is why, different complementary sets of molecules and theoretical approaches were evaluated in ref. 126, but we do describe only the results obtained for Thiel's set herein. First, it was demonstrated that the partially self-consistent *GW* process decreases the impact of the starting XCF on the final BSE/ev*GW* *f* compared to the perturbative BSE/G_0W_0 approach. For instance, for the *s*-triazine, starting with M06-L eigenstates, a meta-GGA free of exact exchange, or M06-2X eigenstates, a GH with 54% of exact exchange, almost doubles the computed *f* at the BSE/G_0W_0 level (from 0.009 to 0.017 for the $1A_2''$ ES, and from 0.200 to 0.357 for the 1E′ ES) whereas it has a significantly milder impact with BSE/ev*GW* (from 0.015 to 0.017 for the $1A_2''$ ES, and from 0.319 to 0.404 for the 1E′ ES). The latter approach also delivers more accurate estimates compared to CC3 (0.016 and 0.386, for the $1A_2''$ and 1E′ ES, respectively).[190] Secondly, the BSE/ev*GW* oscillator strengths were compared to their CC3 and ADC(3/2) counterparts. As can be deduced from the results of Table 5,

Table 4 MAE (in eV) obtained for two specific subsets of dyes and for the total 80-molecule set, considering experimental 0–0 values as references. In the rightmost column, the linear determination coefficient, R^2, for the whole set of compounds is given. Adapted from Table 6 in ref. 125 – see that work for technical details

	MAE			
Method	CT	Cyanine	Total	R^2
ADC(2)	0.20	0.12	0.14	0.92
CC2	0.18	0.19	0.13	0.92
TD-M06-2X	0.24	0.45	0.24	0.90
BSE/ev*GW*@M06-2X	0.17	0.18	0.15	0.91

Table 5 Results of a statistical analysis performed for the BSE/ev*GW*@M06-2X oscillator strengths determined for Thiel's set using the TZVP atomic basis set, considering the CC3/TZVP data of ref. 190 as references. Both absolute (w/o units) and relative (in %) average errors are reported. Adapted with permission from ref. 126, Copyright 2016, American Chemical Society. See that work for details

		Abs. deviations		Rel. deviations	
Method	Set	MSE	MAE	MSE	MAE
BSE/ev*GW*@M06-2X	All	−0.000	0.018	6.7	22.5
	π–π*	−0.003	0.020	8.5	23.4
	n–π*	0.000	0.000	−1.9	20.0
CC2 (ref. 190)	All	0.030	0.033	28.0	32.8
ADC(3/2) (ref. 189)	All	0.019	0.041	2.2	27.5

which reports the absolute and relative errors compared to Kánnár and Szalay's CC3 data,[190] BSE/ev*GW* was found to deliver accurate oscillator strengths for dipole-allowed transitions. Indeed, BSE/ev*GW* is associated with trifling MSE and MAE values, both smaller than the one obtained with CC2 or ADC(3/2). While this result seems spectacular, it might be partially related to the specific sets of compounds considered.

3.3 Charge-transfer transitions

CT excitations, that are central in a wide variety of important processes at the heart of photovoltaics, photocatalysis and photochemistry, constitute a well documented case where TD-DFT may lead to significant errors, especially if local or global hybrid XCF with a rather low exact exchange ratio is used.[192–194] Indeed, TD-DFT calculations with these XCF generally provide very low transition energies for CT states, and, in addition, tend to lead to spurious (non-physical) CT transitions.[195] This problem can be overcome by selecting RSH,[154,184,196] but these XCF tend to overestimate the transition energies for local valence ES, so that simultaneously describing both families of ES is not a cakewalk within the TD-DFT formalism.

The physics of CT excitations, which are excitations for which the promoted electrons and holes left behind do not spatially overlap, can be understood qualitatively by considering the so-called Mulliken limit[197] of a transition from the HOMO of a donor molecule to the LUMO of an acceptor molecule located at a distance R. In the limit of large R, the excitation energy should become $E_{\rm CT}$ = AE − IP − 1/R, where AE is the electronic affinity of the acceptor, IP is the ionization potential of the donor, and $(-1/R)$ is the (attractive) Coulomb electron–hole interaction, with the electron localized on the acceptor and the hole on the donor after photo-excitation. The analysis of the TD-DFT Hamiltonian, eqn (23), indicates that, in a 2-level model and for large electron–hole distance, the transition energy becomes:

$$E_{\rm CT}^{\rm TD\text{-}DFT} = \varepsilon_{\rm L}^{\rm KS} - \varepsilon_{\rm H}^{\rm KS} - \int {\rm d}\mathbf{r}{\rm d}\mathbf{r}' |\phi_{\rm L}(\mathbf{r})|^2 v_{\mu}^{\rm LR}(\mathbf{r},\mathbf{r}') |\phi_{\rm H}(\mathbf{r}')|^2, \quad (24)$$

where (H, L) index the HOMO and LUMO levels and wavefunctions, while $v_{\mu}^{\rm LR}$ is the long-range exact-exchange potential in a RSH formulation with an attenuation parameter of μ. Due to the spatial separation of the hole and electron, the product $\phi_{\rm H}(\mathbf{r})\phi_{\rm L}(\mathbf{r})$ involved in the integrals containing the DFT kernel $K^{\rm HXC}$ tends to zero at large R: the hole and the electron simply do not interact within TD-DFT if the functional does not contain any explicit exact exchange contribution. This simple model outlines the problem faced by TD-DFT, namely the (IP–AE) gap is replaced by its KS ansatz $(\varepsilon_{\rm L}^{\rm KS} - \varepsilon_{\rm H}^{\rm KS})$ and the $(-1/R)$ electron–hole interaction can only be captured by the portion of exact exchange in a GH, or the long-range fraction of exact exchange in a RSH. In particular, if the long-range contribution of exact exchange amounts to, *e.g.* 65%, as in the CAM-B3LYP XCF,[154] the long-range electron–hole attraction will be reduced to $(-0.65/R)$ and the accuracy of the TD-DFT transition energy relies on a compensation of errors between that on the (IP–AE) estimate and that on the long-range electron–hole interaction.

Turning now to the BSE/*GW* scheme and following eqn (21), the same limit becomes:

$$E_{\rm CT}^{{\rm BSE}/GW} = \varepsilon_{\rm L}^{GW} - \varepsilon_{\rm H}^{GW} - \int {\rm d}\mathbf{r}{\rm d}\mathbf{r}' |\phi_{\rm L}(\mathbf{r})|^2 W(\mathbf{r},\mathbf{r}') |\phi_{\rm H}(\mathbf{r}')|^2, \quad (25)$$

with, as discussed above, $(\varepsilon_{\rm L}^{GW} - \varepsilon_{\rm H}^{GW})$ designed to provide an accurate estimate of (AE–IP) and the screened Coulomb potential W reducing to the bare (unscreened) Coulomb potential, so that the W matrix elements reduce correctly to $(-1/R)$ at long distance in a vaccuum, or $(-1/\varepsilon_{\rm M}R)$ in a medium of dielectric constant $\varepsilon_{\rm M}$, that is the physically-correct limit.

The use of BSE calculations to accurately reproduce optical excitations displaying a large CT character was pioneered in the study of organic crystals where low-lying excitations are of hybrid localized and CT character, with a balance between the two limits that strongly depends on the molecular building block (pentacene, picene, *etc.*) and crystallographic structure.[68,70–72,75,77,78]

Concerning gas phase molecules and complexes, the correct behavior of BSE/*GW* for both intramolecular[93,97,99,101,117,118,121] and intermolecular[95,96,98,100,107,114] CT excitations was demonstrated in several studies, including the case of CT excitations from nucleobases to water.[107] As a first illustration, we report in Fig. 8 the example of gas phase donor–acceptor complexes for which experimental data exist and that have been initially used as a benchmark for TD-DFT calculations performed with the optimally-tuned Baer–Neuhauser–Livshits (BNL) RSH.[198] Clearly, the BSE/ev*GW* calculations are accurate as are the TD-BNL calculations. The attenuation parameter (μ) in the BNL XCF is

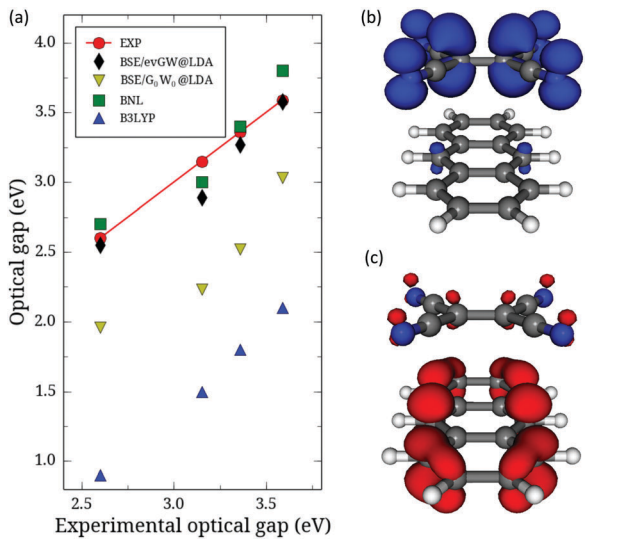

Fig. 8 (a) Comparison of theoretical and experimental absorption onset energy for gas phase donor–acceptor dimers combining tetracyanoethylene (TCNE) with benzene, toluene, *o*-xylene, and naphthalene. These transitions show a strong CT character. While TD-B3LYP yields dramatically too small CT excitation energies, optimally tuned TD-BNL and BSE/ev*GW*@LDA calculations provide reliable estimates. The BSE/G_0W_0 transitions are too small due to the underlying non-selfconsistent G_0W_0@LDA calculations that yield too small a HOMO–LUMO gap (adapted with data from ref. 95 and 198). Representation of the (b) hole-averaged electron density and (c) electron-averaged hole-density for the lowest BSE singlet $\psi_{\lambda=1}^{\rm BSE}(\mathbf{r}_{\rm e},\mathbf{r}_{\rm h})$ excitation in an anthracene–TCNE complex.

optimized to reproduce the correct (IP–AE) gap with a functional form that displays 100% of long-range exact exchange. In contrast, within the BSE formalism, the screened Coulomb potential W is a parameter-free operator that yields the correct electron–hole interaction in all ranges and for any dielectric environment without the need for "tuning".

As stated above, many other demonstrations of the ability of BSE/*GW* to accurately describe CT transitions have appeared. In a 2010 work, Rocca and coworkers demonstrated that BSE gives CT and local excited-states within a few tenths of eV of CASPT2 reference values in a prototypical dipeptide, whereas TD-DFT accurately reproduces the latter but dramatically underestimates the energy of CT transitions when a local XCF is used.[93] This success, obtained starting directly with KS eigenstates corrected by opening the HOMO–LUMO gap to be more physically sound, was confirmed for the same system three years later using more "standard" BSE/*GW* schemes.[99] In 2012, the much larger zinc-bacteriochlorin-bacteriochlorin dimer, that is the original system discussed by Dreuw and Head-Gordon to reveal the limitations of TD-DFT,[194] was investigated[96] and it was found that BSE/*GW* provides CT transition energies close to the one obtained with TD-CAM-B3LYP,[199] that is much more accurate than the TD-DFT ones obtained with local functionals or global hybrids.[194,199] Of course, beyond those "toy" systems, more realistic cases have also been tackled. In 2012, Baumeier *et al.* studied dicyanovinyl-substituted oligothiophenes showing internal acceptor–donor–acceptor character and concluded that BSE nicely reproduces experimental data with increasing number of central thiophene units (see Fig. 9) with a better agreement when going beyond the Tamm–Dancoff approximation.[97] In 2016, Ziaei and Bredow studied three large CT compounds used in thermally-activated delayed-fluorescence and obtained highly accurate BSE energies for all three systems, using an underlying *GW* approach in which the orbital energies in G are updated and W is frozen to its starting W_0 value.[114] Likewise the same authors have found a good match between BSE/*GW* and experimental results in a donor–acceptor

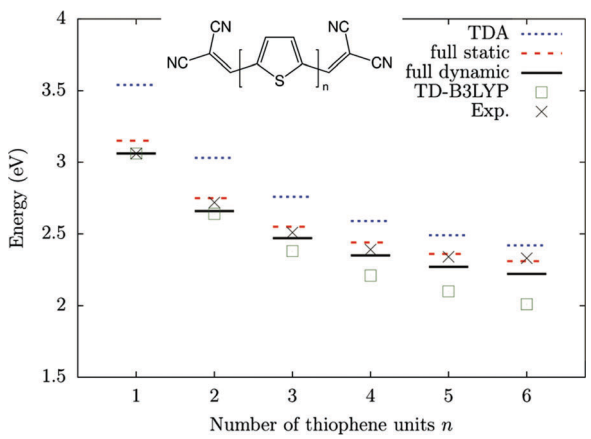

Fig. 9 Evolution with the number of thienyl units (n) of the absorption energies of the substituted oligomers showed at the top, using TD-B3LYP (empty squares) and various BSE/*GW* variants (full, dashed and dotted lines). The experimental values are given as crosses. Adapted with permission from ref. 97. Copyright 2012 – American Chemical Society.

complex composed of a large central macrocycle substituted by two perylene-bis-imide moieties, whereas the TD-DFT results were strongly XCF-dependent for the same compound.[121]

Further, new "tools" have also been developed to extract more information from BSE calculations. On the one hand, paralleling the CT analysis models that have been designed for TD-DFT[200–202] and ADC,[203] Hirose, Noguchi and Sugino have recently set up a protocol to characterize the exciton as local, charge-transfer, Rydberg, *etc.* within the BSE/*GW* formalism.[118] On the other hand, Wehner and Baumeier developed an approach[117] to quantify excitonic couplings in intermolecular CT cases, building on the diabatization techniques pioneered by Kaczmarski and coworkers in the BSE framework for the study of the retinal chromophore ES surface.[92] Such studies open the door to the study of exciton motion or energy transfer processes between molecular units, a formidable field to be explored with the present BSE formalism. Besides applications, these works certainly constitute useful steps to obtain more insightful analyses of the results given by BSE/*GW* calculations.

Finally, as a concluding remark for this section, the need to go beyond local kernels, within both BSE or TD-DFT with hybrid functionals, was also clearly demonstrated in the study of simple inorganic semiconductors such as silicon[204,205] where the large average distance between holes and electrons in the so-called Wannier excitons required as well a proper description of long-range electron–hole interactions, bridging the problematics that quantum chemists and solid-state physicists were facing.

3.4 Cyanine dyes

Cyanine derivatives, in which a positive or negative (formal) charge is delocalized over a π-conjugated unit containing an odd number of atoms, are of prime importance in dye chemistry. This is because these compounds allow simultaneously achieving redshifted absorption and emission wavelengths together with extremely large extinction coefficients. For instance, one of the most popular fluorophores, namely BODIPY, can be viewed as a *cis*-constrained cyanine.[206] It is well-recognized that TD-DFT has difficulties in providing accurate transition energies for these systems,[207–210] a problem for which the current state-of-the-art has been summarized in a 2015 review.[20] In short, irrespective of the selected XCF (semilocal, GH or RSH), the TD-DFT transition energies tend to be too large, contrasting therefore with the CT cases for which TD-DFT tends to underestimate these energies. This is due to a particularly strong electronic reorganization when going from the GS to the ES: differential electronic correlation effects are large. While wave-function approaches accounting for dynamical correlation, such as ADC(2),[211] CC2[209] and CASPT2,[207,209] are able to capture these effects, TD-DFT fails to do so.

First, for the prototypical model streptocyanine chains of increasing length (see top of Fig. 10), it was shown that the BSE/ev*GW* transition energies are very close to reference CC3 values,[209] with deviations systematically smaller than 0.1 eV for chains containing between 3 and 9 carbon atoms.[105] As can be seen in Fig. 10, the BSE/ev*GW* values are, in addition, bracketed by the multi-reference CASPT2 and diffusion Monte-Carlo data (DMC)

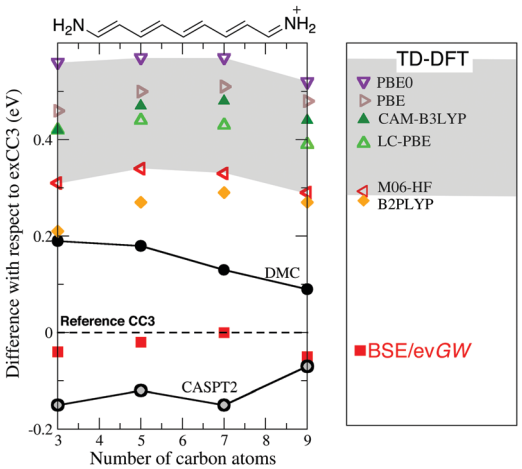

Fig. 10 Evolution with chain length of the error (in eV) in the lowest excitation energy of streptocyanine derivatives obtained with several methods, considering the CC3 data as reference. The circles represent wavefunction approaches, the triangles and diamonds TD-DFT results, whereas the squares correspond to BSE/ev*GW* data. Adapted with permission from ref. 105, Copyright 2016, American Chemical Society.

and are clearly much more accurate than TD-DFT values, even when the double-hybrid B2PLYP XCF is selected.[212] This success has motivated further applications of the BSE/ev*GW* theory aiming to reproduce the experimental 0–0 energies of "real-life" cyanine derivatives, namely fluoroborate derivatives[104] and arylcarbonium dyes,[127] using protocols similar to the one applied in the 80-molecule 0–0 benchmark described in Section 3.1.[125] In the former study, the MAE obtained with TD-DFT attains 0.42 eV for a set of 10 BF_2-bearing dyes, and this error could be divided by almost a factor of three when using BSE/ev*GW* (0.15 eV).[104] In the second work, two substituted Michler's hydrol blue and three acridine cationic compounds were described with TD-DFT, ADC(2) and BSE/ev*GW* considering a palette of environmental models.[127] It was concluded that the former method systematically overestimates the transition energies, whereas the two latter provide much more accurate values. Despite the relatively small number of molecules treated up to now, it seems therefore rather clear that BSE can be advantageously applied to model cyanine transitions.

3.5 Triplet excitations

Owing to the similarities between the BSE, TD-DFT and TD-HF formalisms, with BSE standing as a time-dependent screened-exchange approach, the question of the Hartree–Fock triplet instability, and its consequences on TD-DFT triplet calculations,[23,213–215] is clearly expected to impact the calculation of triplet excitation energies within BSE. In fact, complementing the benchmarks performed for singlet excitation energies over Thiel's set of molecules and transitions,[123,124] similar studies were performed for triplet excitations in comparison with quantum chemistry wavefunction methods.[128,129] As shown in Fig. 5, the MSE for the triplet transitions in Thiel's set was found to be as large as *ca.* −0.6 eV when a BSE/G_0W_0 approach that provided excellent singlet excitation energies was adopted, that is, when the KS eigenstates generated with a XCF containing a significant amount of exact exchange were used as input.[124,129] Similar underestimations of the reference triplet energies were disappointedly reported when considering BSE/ev*GW*, starting with various hybrid XCF,[128,129] namely when using a BSE approach shown to yield small errors for singlet excitations.[123,129] Clearly, at least in Thiel's set of molecules, the BSE formalism yields triplet excitation energies that are too low as compared to the corresponding singlets, yielding too large singlet–triplet splittings, $\Delta_{S_1-T_1}$, a parameter of prime importance in third-generation phosphors relying on thermally activated delayed fluorescence. Whether these large errors found for small compounds do pertain in larger molecules remains however an open question.

Following previous analyses carried out within the TD-DFT framework,[23,213–215] the application of the Tamm–Dancoff approximation,[213] namely the neglect of the non-resonant (C) blocks in the eigenvalue problem of eqn (20), was found to generally improve the calculation of triplets with BSE, by inducing a *ca.* 0.15 eV blueshift of their energy,[128,129] an effect presenting a sign and magnitude similar to the one found in TD-DFT. However, since the Tamm–Dancoff approximation also induces a blueshift of the BSE singlet excitation energies, the $\Delta_{S_1-T_1}$ splittings are not significantly improved, with an error of the order of *ca.* 0.2–0.3 eV for both the full-BSE/ev*GW* and the TDA-BSE/ev*GW* calculations.[128] This is illustrated in Fig. 11 in the case of BSE/ev*GW*@M06-2X calculations for Thiel's set. With full-BSE, the singlets are accurately described and the triplets significantly too low, whereas with TDA one improves the description of the triplets (though not sufficiently), at the cost of degrading the accuracy for singlets. However, it is noteworthy that for acenes, the TDA completely removes the triplet instability that occurs with increasing number of rings,[129] with an evolution of the BSE (T_1/T_1^{TDA}) ratio with oligomeric length that is reminiscent of that obtained with RSH.[215] Nevertheless, for pentacene, the TDA $\Delta_{S_1-T_1}$ splitting still remains very large, *ca.* 0.2 eV.[129] More generally, for the acene series, it was also found that the accuracies provided by BSE or TDA-BSE for singlet and triplet excited-states significantly differ.[84]

Within a TD-DFT approach relying on range-separated hybrids, the amount of short or long-range exchange, and the

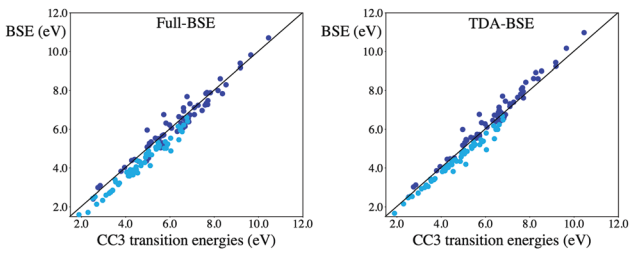

Fig. 11 Comparisons between the CC3 and BSE/ev*GW*@M06-2X (left) and TDA-BSE/ev*GW*@M06-2X (right) panel for the singlet (dark blue) and triplet (light blue) excitation energies in Thiel's set. The central line indicates a perfect match. All values are obtained with the TZVP atomic basis set. Adapted with permission from ref. 128, Copyright 2016, American Chemical Society.

attenuation parameter, can be tuned, providing flexibility to simultaneously optimize the HOMO–LUMO gap, the S_1 energy as well as the S_1–T_1 energy splitting.[215] Within the BSE/*GW* formalism, the screened Coulomb potential W can only be marginally tuned by varying the input KS eigenstates. As a consequence, the calculation of accurate triplet energies and singlet–triplet energy splittings within BSE stands as a challenge to the community.

3.6 Further applications

Besides benchmark works and investigations focussed on a class of excitations, there have been several BSE/*GW* studies devoted to more specific cases and we will briefly describe some of these works. In 2014, Noguchi and coworkers investigated the firefly luciferin anion, a hallmark chromogen of bioluminescence.[106] As can be seen in Fig. 12, these authors found that the BSE/G_0W_0 approach could nicely reproduce the experimental line shapes for both Rydberg (sky blue background) and resonant (yellow background) excitations, though the BSE spectra were 0.5 eV blueshifted compared to experiment. TD-B3LYP was found less accurate in these spectral regions. For the lower lying excitations (white background), the agreement was less obvious, though it appeared that TD-B3LYP was probably more suited to describe that spectral domain.[106] Coccia *et al.* performed a detailed analysis of the geometrical and optical signatures of a model carotenoid combining variational Monte Carlo to obtain accurate bond length alternation (BLA) and BSE to model both the B_u and A_g-like excited-states of this polyene.[103] They notably showed that the dependence of the former ES energy on the BLA was enhanced in BSE compared to TD-DFT. The same group investigated other biological chromogens in various environments in further works.[102,216] In 2017, Noguchi and Sugino investigated a series of cycloparaphenylenes (CPP) containing between 3 and 16 units at the BSE/G_0W_0 level.[120] They reached very good agreement between their simulated UV/Vis spectra and the experimental measurements irrespective of the considered CPP size, allowing a careful analysis of the nature of the involved ES. They concluded that the optical spectra of these compounds can be analyzed in terms of their nodal structures and that, starting from the decamer, the nature of the excited-state becomes rather insensitive to the CPP size.

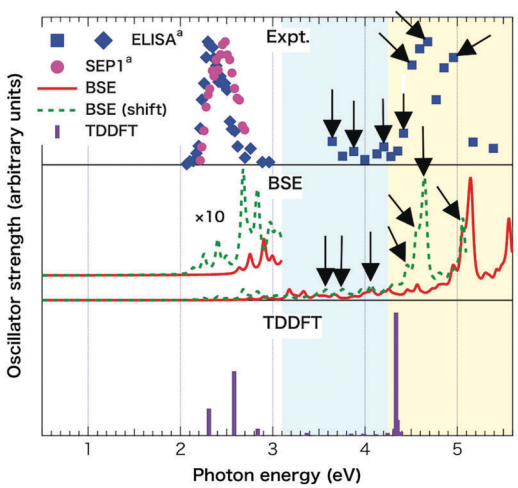

Fig. 12 Top: Experimental measurements for the firefly luciferin anion in the gas phase. Center: Non-shifted (red line) or 0.5 eV shifted (green dotted line) BSE spectrum. Bottom: Stick TD-B3LYP spectrum. Reproduced with permission from ref. 106, Copyright 2014, American Institute of Physics.

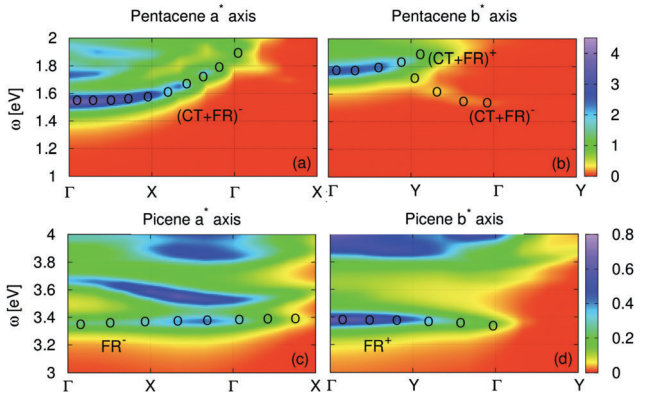

Fig. 13 Map of the imaginary part of the macroscopic dielectric function ε_2 evaluated as a function of the energy (vertical axis) and momentum transfer (horizontal axis) along (a) the *a** and *b** axis of pentacene and picene. Black circles are guides to the eye for the lowest energy excitons. $(CT + FR)^{\pm}$ are symmetric/antisymmetric mixed (coupled) Frenkel and CT excitations. Reprinted with permission from ref. 78. Copyright (2013) by the American Physical Society.

Concerning the optical properties of molecular solids, several studies emphasised the interplay between localised (Frenkel) and charge-transfer excitations as probed by optical experiments,[68,70–72,75,77,78,83] revealing on the one hand, that the character of optical excitations is driven by the electron and hole hopping energies from one site to another and, on the other hand, by the electron–hole interactions composed of the direct screened interaction and bare exchange terms (see eqn (21)). Beyond "zone-center" optical excitations, Cudazzo and coworkers[78] further explored the dispersion of the excitations as a function of the electron–hole center of mass momentum, a well-defined quantity in periodic systems (see Fig. 13). Such a study provided a way to revisit, at the BSE level, the physics of singlet fission in organic solids such as pentacene,[84,217] with a novel mechanism unravelling the decay of zone-center ($Q = 0$) singlet excitations into two triplet excitations with opposite (Q) and ($-Q$) momentum.[217]

Targeting now photovoltaic applications, calculations by Baumeier and coworkers[98] emphasized the strong impact of the donor and acceptor relative molecular orientation on the energy difference between the lowest S_1 excitation energy of the donor and the lowest CT excitation, with the conclusion that the geometry at the donor–acceptor interface in bulk-heterojunction solar cells can dramatically affect the electrostatic energy profile, enhancing or impeding the electron–hole dissociation (for larger scale electrostatic studies, see *e.g.* ref. 218). As yet another example, Gala and coworkers studied a substituted oligothiophene used in bulk-heterojunction solar cells,[112] and determined the properties of π-stacked dimeric structures of these

oligomers. They found that the experimental spectrum could not be reproduced by accounting only for one molecule, and that a better accuracy was obtained when considering the dimer, which is consistent with the fact that intermolecular optical transitions play a significant role.

More recently, BSE/*GW* investigations of large photoactive molecules grafted onto nanoparticles appeared.[115,122] In ref. 115, targeting photovoltaic applications, the authors studied a well-known push–pull dye (JK2) anchored onto TiO_2 using a plane-wave approach and obtained extremely good agreement between theory and experiment for all relevant gaps and potentials, which was a significant improvement compared to all previous (TD-)DFT attempts. In ref. 122, BSE/ev*GW* was used as a reference to select an accurate functional for TD-DFT simulations of an azobenzene photochrome grafted onto a TiO_2 nanoparticle. Indeed, in such a system, there is a competition between electron injection into the TiO_2 conduction band and photochromism once the *trans*-azobenzene has been excited, and the selection of a specific XCF has a qualitative impact on TD-DFT's prediction, leading to an incertitude that could be lifted thanks to BSE calculations.

4 Environmental effects: embedded BSE implementations

As indicated in the Introduction, the tremendous success of TD-DFT has been certainly accelerated by the development of embedding techniques, within either the continuum model, such as the well-known polarizable continuum model (PCM) of the Pisa group,[7–9,219] or various discrete polarizable models (DPM)[6,10,11,220–222] that all rely on the partitioning of the atoms in several subsets treated at different theoretical levels, which constitutes the basis of the QM/MM techniques. Indeed, besides gas phase and periodic boundary calculations, these embedding techniques allow quantum mechanical calculations of photoactive molecules, accounting for the electrostatic and dielectric (polarization) effects induced by the surroundings, *e.g.*, a solvent, an organic matrix, a metallic electrode, a protein, *etc.*

The seminal developments for merging the *GW* and BSE formalisms with embedding techniques originated from a panel of studies aiming at understanding the properties of organic molecules interacting with metallic surfaces.[51,52,223–225] The strong change in the electronic properties of a molecule interacting with a metal, in relation with the "image-charge" that stabilizes electrons and holes injected during a photoemission or transport experiment, stimulated the development of such hybrid techniques. Indeed, *GW* and BSE calculations performed by explicitly considering all electrons in molecular systems adsorbed onto surfaces remain computationally expensive.

The change of the electronic properties induced by the environment might have several origins: (i) ground-state (GS) "crystal" field effects associated with the electrostatic field generated by the environment; (ii) dispersion effects associated with the hybridization of the electronic wavefunctions of the considered compound with those of the environment, and (iii) dynamical polarization effects describing the response of the environment electronic cloud to the (fast) excitation in the QM subsystem during a photoemission or optical excitation. Since hybridization and delocalization effects cannot be treated by combining the QM treatment with a classical (discrete or continuous) environment, but only by including a sufficiently large portion of the environment into the QM subsystem, we will not discuss this aspect further.

The first effect, purely electrostatic and related to the GS, can be easily captured within DFT using the standard implementations available in many quantum chemistry codes. In the case of solutes, the effect of the fluctuating solvent molecules' dipolar or quadrupolar fields can be either described by QM/MM techniques combined with classical (force-field) molecular dynamics, or with the PCM formalism relying on a dielectric constant that accounts for the (slow) relaxation of all (nuclei + electron) degrees of freedom, *e.g.*, by using $\varepsilon_0 = 78.39$ in water. Since the BSE/*GW* schemes require KS eigenstates as an input, many-body calculations starting with embedded DFT calculations will naturally capture these GS electrostatic effects. This strategy was exploited by Varsano and coworkers in their BSE studies of chromophores inside a realistic biological environment.[102,103,216]

The third effect, that is the dynamical (fast) electronic response of the surrounding medium, can be incorporated into the *GW* and BSE formalisms by ensuring that the screened Coulomb potential W that acts on the QM subsystem accounts for the dielectric response of both the QM and MM (or PCM) environment. Formally, since there is no hybridization between the two subsystems, one can show that the QM and MM independent-electron susceptibilities just add up, straightforwardly leading to the result that environmental polarization effects are fully included in the screened Coulomb potential W build from eqn (8) provided that the bare Coulomb potential v is dressed with the environment reaction field, that is: $v \rightarrow v + v^{\mathrm{reac}}$ with $v^{\mathrm{reac}} = v\chi^{\mathrm{MM}}v$, where χ^{MM} is the susceptibility of the MM (or PCM) subsystem. Such a renormalisation technique of the W potential was also applied to study the electronic properties of inorganic systems, including nanotubes in bundles[226] or stacks of 2D layers[227] within the so-called $G\mathrm{d}W$ approach.[223]

The inclusion of the surrounding medium dielectric contribution into the screened Coulomb potential W, and the related effects on the *GW* electronic energy levels and BSE optical spectra, was pioneered in quantum chemistry by Baumeier and coworkers, who described the environment as a grid of polarizable centers reproducing, *via*, *e.g.*, the Clausius–Mossotti relation, the proper environmental (optical) dielectric response (see Fig. 14).[101] They specifically showed that the energy ordering of localized and charge-transfer (CT) excitations at donor/acceptor interfaces could be significantly altered by medium effects, with important consequences on the electron–hole pair separation mechanisms which is central in photovoltaic applications. Subsequently, the merging with the PCM and *GW* formalisms was achieved,[228] demonstrating that the *GW* electronic energy levels could accurately capture the very large variations of the ionization potential and electronic affinity for DNA nucleobases immersed in water within a state-specific

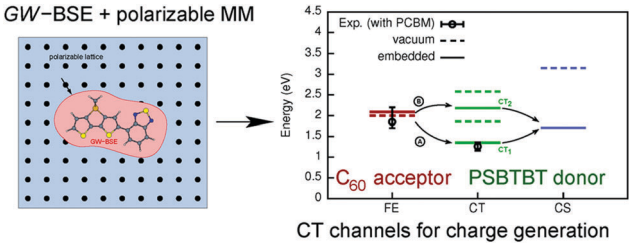

Fig. 14 Pioneering QM/MM implementation of *GW*/BSE. (left) Partitioning into the QM (pink) and MM (blue) subsystems, with a regular grid of polarizable centers in the classical environment reproducing the correct dielectric constant. (right) Renormalisation by the polarizable environment of localized and charge-transfer (CT) optical excitation energies in a paradigmatic donor/acceptor complex of interest for photovoltaics. Reprinted with permission from ref. 101. Copyright 2014 American Chemical Society.

non-equilibrium approach, discriminating properly between the dielectric response of water for GS slow degrees of freedom ($\varepsilon_0 = 78.39$) and fast optical response ($\varepsilon_\infty = 1.78$) to the charged excitations.[229] Further, QM/MM implementations of the *GW* and Bethe–Salpeter formalisms, with an atomistic description of the environment including both static field and dynamical polarization, were developed for the treatment of purely organic semiconductors,[230] organic dopants in an organic semiconductor,[231] and polymers in explicit solvents prepared with classical MD simulations.[142]

We conclude this section by emphasizing that existing combinations of the *GW* and BSE formalisms with polarizable models have relied so far on the inclusion of the low-frequency optical dielectric response of only the surrounding medium, neglecting its full energy dependence in the optical range and beyond. While the existing tests and applications mentioned above suggest that this is a valuable approximation, the BSE/*GW* approach offers much more flexibility than, *e.g.*, TD-DFT, to account for the full dynamical response by defining a frequency dependent reaction field built from the dynamical effective medium susceptibility $v^{\mathrm{reac}}(\omega) = v\chi^{\mathrm{MM}}(\omega)v$. The use of simple plasmon-pole models for the environment dielectric response may be a first step in that direction.

5 Challenges

Besides the triplet problem mentioned above, several challenges are still ahead of the Bethe–Salpeter community to gain some of the visibility and wide usage that the TD-DFT formalism is enjoying. While many aspects could be mentioned, we emphasize first an important practical aspect, namely the ability to calculate analytic forces in the excited states, which is now usual in many TD-DFT implementations but remains to be achieved at the BSE/GW level. Further, two more fundamental issues, aiming at bridging the gap with reference wavefunction quantum chemistry techniques, concern the ability to tackle transitions with multiple excitation character, and the existence of a clear path for systematic improvements, both being commonly found in single-reference quantum chemistry methods such as CC and ADC techniques.

5.1 Analytic forces and energy surfaces in the excited state

The study of light emission (fluorescence, phosphorescence) requires the ability to perform structural relaxations in the excited state. However, while analytic forces in the excited states have been implemented within TD-DFT,[13,14,232–236] the formalism for analytic BSE forces remains to be derived and implemented. Besides expensive finite difference calculations, a seminal exploration in the field was performed by Ismail-Beigi and Louie under the approximation that one can neglect the impact of displacing the nuclei positions on the screened Coulomb potential, that is $(\partial W/\partial R_I) = 0$, in the derivation of the ES energy $(\partial E_\lambda/\partial R_I)$ gradients. This approximation was validated in the case of the small CO and NH_3 molecules by comparison with explicit finite-difference calculations, an approximation later corroborated by applying the same approximation in the calculation of the gradient of the *GW* energy levels.[237,238] However, much larger test sets on more realistic systems are still to be carried out for better assessing the error introduced by assuming the stationarity of W. Further, as recently shown in the case of deriving analytic forces within the RPA formalism,[239] the use of real-space-grid and (imaginary) time formalisms allows obtaining simple expressions for the derivative of the susceptibility, opening the door to manageable expressions for the gradients of W.

5.2 Beyond the adiabatic approximation and multiple excitations

A serious and well-known TD-DFT limitation is the standard adiabatic approximation, namely the assumption that the exchange–correlation potential $v_{\mathrm{xc}}(t)$ is local in time, that is it depends only on the charge density $n(t)$ at the same time (t), and not on charge densities $n(t')$ at earlier times, washing out memory effects. While going beyond the adiabatic approximation within TD-DFT remains as a challenge,[240,241] the *GW* and BSE formalisms straightforwardly include memory effects as they rely on the dynamical susceptibility $\chi(\omega)$ and the related dynamically screened Coulomb potential $W(\omega)$. However, in practice, standard BSE calculations impose the adiabatic approximation for numerical tractability purposes, namely using only the low-frequency limit $W(\omega = 0)$. As such, the formalism for going beyond the adiabatic approximation within BSE exists, and it is a matter of computational efficiency that limits its use. Calculations with a dynamical W have been performed on realistic systems such as rhodopsin and yellow proteins within a simplified analytic ''plasmon-pole'' description of the dynamics of the dielectric response, typically leading to red-shifts of up to 0.3 eV for the n–π* transition energies compared to adiabatic calculations.[90] The effect was however found to be much smaller in the case of π–π* transitions.[90,97] Further, a *ca.* 0.3 eV redshift was found in the case of the triplet excitations of sexithiophene molecules, a dynamical shift reduced however to 0.1 eV for singlet excitations.[82] Besides potentially providing an improved description of ''standard'' optical excitations, going beyond the adiabatic approximation should possibly allow tackling multiple excitations, as discussed both within

the TD-DFT[242,243] and BSE frameworks.[244–246] Concerning the connections between TD-DFT and BSE, it is worth mentioning that Romaniello and coworkers precisely constructed a dynamical kernel for TD-DFT by mapping the 4-body BSE dynamical response function L onto the 2-body standard susceptibility χ response function,[243] illustrating the interplay between these two methods that may emerge in the future. Alternatively, Rebolini and Toulouse[246] used a range-separated approach to combine standard adiabatic TD-DFT in the short range and dynamical Bethe–Salpeter in the long range, providing another direction for combining these two techniques and improving their accuracy-to-cost ratio.

5.3 Is there a systematic path to accuracy improvement?

As emphasized above, the standard BSE formalism offers a very good compromise between computer cost and accuracy, with a reliable description of localized, charge-transfer, cyanine-like, Rydberg, *etc.* excitations, and a scaling with system size, in terms of computational cost requirements, identical to TD-DFT. A potential advantage of the BSE formalism, as compared to TD-DFT, is that it relies on perturbation theory, offering thus in principle a pathway to improve the accuracy by including higher order terms at the cost of increased computational efforts. In the *GW* and BSE community, higher order contributions in terms of the screened Coulomb potential are labelled vertex corrections,[47,247] and pioneering studies on their impact at both the *GW* and BSE levels have recently appeared for molecular systems.[248,249] The results were somehow mitigated. Maggio and Kresse[249] emphasized the need to combine full self-consistency with vertex corrections, as known in the case of inorganic systems,[250] which goes on a par with recent reports showing that full self-consistency without vertex corrections leads to rather poor *GW* results.[140,163] Hung and coworkers[248] advocated a different treatment at the *GW* level for occupied and virtual states before proceeding with BSE calculations. Therefore, it is yet too early to conclude that there is a systematic way to significantly improve the accuracy of BSE results as compared to simple pragmatic approaches such as the optimization of starting Kohn–Sham functional, or the self-consistency on the eigenvalues only when starting from standard global hybrids such as PBE0 or M06-2X.

6 Summary

The present Review illustrates that the Bethe–Salpeter formalism may stand as a valuable alternative to TD-DFT for the community of chemists studying the properties of chemical systems of interest for photovoltaic applications, light-emitting devices, photocatalysis, fluorescence, *etc.* As compared to TD-DFT in the so-called Casida's formulation, the BSE formalism presents the same familiar eigenstate representation in terms of single-electron transitions between occupied and virtual molecular orbitals, with the same computer-time scaling with system size that enables the study of systems containing a few hundred atoms. Further, recent implementations based on standard Gaussian atomic basis sets and resolution-of-identity techniques allow its straightforward use by the quantum chemistry community, leading to fair comparisons with the DFT and wavefunction methods currently used by this community. However, and beyond similarities, the BSE formalism relies on different expressions for the constitutive matrix elements, with the inclusion of proper addition and removal electron energies and non-local screened Coulomb interactions between electrons and holes. These differences allow solving some of the well-known problems that TD-DFT is facing with in particular more accurate charge-transfer, cyanine or Rydberg excitations, while providing for localized (Frenkel) excitations a similar accuracy as the one obtained with the best TD-DFT or second-order wavefunction methods, such as, ADC(2), CC2 and, even in some cases, CASPT2. Importantly, such a reliability is obtained with an approach that suffers much less from the functional dependency that complicates the use of TD-DFT for studying unknown systems or compounds in which several excited-states of different nature play a role. Such a starting point insensitivity can be easily obtained by using *GW* addition or removal energies obtained either using simple partial self-consistent schemes such as ev*GW*, or by tuning the starting DFT functional such that the Kohn–Sham and resulting *GW* spectra (ionization energy, HOMO–LUMO gap, *etc.*) agree, two schemes that do not require any experimental input.

Concerning upcoming developments, we emphasized that the BSE formalism relies on a many-body Green's function formalism that provides a documented way to include dynamical effects, namely memory effects, beyond the standard adiabatic approximation, offering a potential path to the study of transitions with multiple excitation character. Further, the inclusion of higher order terms, labeled vertex corrections, should allow in principle systematic improvements of the accuracy, at the cost certainly of increased computational requirement. It is however too early to conclude that such a development may result in a formalism that can compete with the accuracy-to-cost ratio that is attained with *e.g.* coupled-cluster techniques that provide a well defined path to accuracy with increasing order.

While the BSE formalism can be straightforwardly implemented in a TD-DFT code once the (static) screened Coulomb potential and *GW* energy levels are obtained, it remains that the *GW* calculation of the true electron addition/removal energies, as calculated within photoemission, stands as the main bottleneck in terms of implementation and computer cost, even though presenting also an $\mathcal{O}(N^4)$ scaling with standard resolution-of-identity techniques. Still, the *GW* formalism has now been implemented in several well-known Gaussian-based generalist quantum chemistry codes, such as Turbomole[168] and CP2K,[251] or dedicated codes,[140,165,166,252] notwithstanding historical planewave implementation in codes such as VASP. Further, clever algorithms are starting to pave the way to *GW* calculations with reduced cost and scaling,[54,115,170–172,253] highlighting the potential for an increasing popularity in the quantum chemistry community.

Conflicts of interest

There are no conflicts to declare.

Acknowledgements

The authors are indebted to the collaborators who contributed to the developments and applications of the BSE formalism in their groups: Claudio Attaccalite (CNRS, Grenoble), C. Azarias (Nantes), David Beljonne (Mons), Paul Boulanger (CNRS, Grenoble), Gabriele D'Avino (Mons and CNRS Grenoble), D. Escudero (Nantes), Carina Faber (CNRS, Grenoble), Jing Li (CNRS, Grenoble), and Valerio Olevano (CNRS, Grenoble). Gian-Marco Rignanese and Jing Li are warmly acknowledged for helping with Fig. 1 and 8.

References

1 C. J. Stein and M. Reiher, *J. Chem. Theory Comput.*, 2016, **12**, 1760–1771.
2 S. Shirai, Y. Kurashige and T. Yanai, *J. Chem. Theory Comput.*, 2016, **12**, 2366–2372.
3 M. E. Casida, in *Time-Dependent Density-Functional Response Theory for Molecules*, ed. D. P. Chong, World Scientific, Singapore, 1995, vol. 1, pp. 155–192.
4 C. Ullrich, *Time-Dependent Density-Functional Theory: Concepts and Applications*, Oxford University Press, New York, 2012.
5 D. Jacquemin and C. Adamo, in *Computational Molecular Electronic Spectroscopy withTD-DFT*, ed. N. Ferré, M. Filatov and M. Huix-Rotllant, Springer International Publishing, Cham, 2016, vol. 368, pp. 347–375.
6 D. Jacquemin, B. Mennucci and C. Adamo, *Phys. Chem. Chem. Phys.*, 2011, **13**, 16987–16998.
7 M. Caricato, B. Mennucci, J. Tomasi, F. Ingrosso, R. Cammi, S. Corni and G. Scalmani, *J. Chem. Phys.*, 2006, **124**, 124520.
8 R. Improta, G. Scalmani, M. J. Frisch and V. Barone, *J. Chem. Phys.*, 2007, **127**, 074504.
9 A. V. Marenich, C. J. Cramer, D. G. Truhlar, C. G. Guido, B. Mennucci, G. Scalmani and M. J. Frisch, *Chem. Sci.*, 2011, **2**, 2143–2161.
10 D. Presti, F. Labat, A. Pedone, M. J. Frisch, H. P. Hratchian, I. Ciofini, M. C. Menziani and C. Adamo, *J. Chem. Theory Comput.*, 2014, **10**, 5577–5585.
11 D. Presti, F. Labat, A. Pedone, M. J. Frisch, H. P. Hratchian, I. Ciofini, M. Cristina Menziani and C. Adamo, *J. Comput. Chem.*, 2016, **37**, 861–870.
12 Z. Rinkevicius, I. Tunell, P. Salek, O. Vahtras and H. Ågren, *J. Chem. Phys.*, 2003, **119**, 34–46.
13 C. van Caillie and R. D. Amos, *Chem. Phys. Lett.*, 1999, **308**, 249–255.
14 F. Furche and R. Ahlrichs, *J. Chem. Phys.*, 2002, **117**, 7433–7447.
15 G. Scalmani, M. J. Frisch, B. Mennucci, J. Tomasi, R. Cammi and V. Barone, *J. Chem. Phys.*, 2006, **124**, 094107.
16 J. Liu and W. Z. Liang, *J. Chem. Phys.*, 2011, **135**, 014113.
17 F. Santoro and D. Jacquemin, *Wiles Interdicip. Rev.: Comput. Mol. Sci.*, 2016, **6**, 460–486.
18 M. E. Casida and M. Huix-Rotllant, *Annu. Rev. Phys. Chem.*, 2012, **63**, 287–323.
19 A. D. Laurent and D. Jacquemin, *Int. J. Quantum Chem.*, 2013, **113**, 2019–2039.
20 B. Le Guennic and D. Jacquemin, *Acc. Chem. Res.*, 2015, **48**, 530–537.
21 L. Goerigk, J. Moellmann and S. Grimme, *Phys. Chem. Chem. Phys.*, 2009, **11**, 4611–4620.
22 L. Goerigk and S. Grimme, *J. Chem. Theory Comput.*, 2011, **7**, 3272–3277.
23 M. J. G. Peach, M. J. Williamson and D. J. Tozer, *J. Chem. Theory Comput.*, 2011, **7**, 3578–3585.
24 M. J. G. Peach and D. J. Tozer, *J. Phys. Chem. A*, 2012, **116**, 9783–9789.
25 M. J. G. Peach, N. Warner and D. J. Tozer, *Mol. Phys.*, 2013, **111**, 1271–1274.
26 A. Prlj, B. F. E. Curchod, A. Fabrizio, L. Floryan and C. Corminboeuf, *J. Phys. Chem. Lett.*, 2015, **6**, 13–21.
27 O. Christiansen, H. Koch and P. Jørgensen, *Chem. Phys. Lett.*, 1995, **243**, 409–418.
28 O. Christiansen, H. Koch and P. Jørgensen, *J. Chem. Phys.*, 1995, **103**, 7429–7441.
29 K. B. Wilberg, A. E. de Oliveria and G. Trucks, *J. Phys. Chem. A*, 2002, **106**, 4192–4199.
30 M. Caricato, *J. Chem. Theory Comput.*, 2012, **8**, 4494–4502.
31 L. Cederbaum, G. Hohlneicher and S. Peyerimhoff, *Chem. Phys. Lett.*, 1971, **11**, 421–424.
32 J. Schirmer, L. S. Cederbaum and O. Walter, *Phys. Rev. A: At., Mol., Opt. Phys.*, 1983, **28**, 1237–1259.
33 A. Dreuw and M. Wormit, *Wiles Interdicip. Rev.: Comput. Mol. Sci.*, 2015, **5**, 82–95.
34 C. Hättig and F. Weigend, *J. Chem. Phys.*, 2000, **113**, 5154–5161.
35 E. G. Hohenstein, S. I. L. Kokkila, R. M. Parrish and T. J. Martnez, *J. Chem. Phys.*, 2013, **138**, 124111.
36 L. Hedin, *Phys. Rev.*, 1965, **139**, A796–A823.
37 W. Kohn and L. J. Sham, *Phys. Rev.*, 1965, **140**, A1133–A1138.
38 P. C. Martin and J. Schwinger, *Phys. Rev.*, 1959, **115**, 1342–1373.
39 F. Aryasetiawan and O. Gunnarsson, *Rep. Prog. Phys.*, 1998, **61**, 237–312.
40 G. Onida, L. Reining and A. Rubio, *Rev. Mod. Phys.*, 2002, **74**, 601–659.
41 B. Farid, in *Electron correlation in the solid state*, ed. N. March, Imperial College Press, London, 1999, ch. 3, pp. 103–252.
42 R. M. Martin, L. Reining and D. M. Ceperley, *Interacting Electrons: Theory and Computational Approaches*, Cambridge University Press, Cambridge, UK, 2016.
43 G. Strinati, H. J. Mattausch and W. Hanke, *Phys. Rev. Lett.*, 1980, **45**, 290–294.
44 M. S. Hybertsen and S. G. Louie, *Phys. Rev. B*, 1986, **34**, 5390–5413.
45 R. W. Godby, M. Schlüter and L. J. Sham, *Phys. Rev. B: Condens. Matter Mater. Phys.*, 1988, **37**, 10159–10175.
46 W. von der Linden and P. Horsch, *Phys. Rev. B: Condens. Matter Mater. Phys.*, 1988, **37**, 8351–8362.
47 M. Shishkin and G. Kresse, *Phys. Rev. B*, 2007, **75**, 235102.
48 Y. Ping, D. Rocca and G. Galli, *Chem. Soc. Rev.*, 2013, **42**, 2437–2469.

49 We exclude from this statement strongly correlated systems, such as Mott insulator systems, for which the standard one-body picture of band structure breaks down.
50 G.-M. Rignanese, X. Blase and S. G. Louie, *Phys. Rev. Lett.*, 2001, **86**, 2110–2113.
51 J. B. Neaton, M. S. Hybertsen and S. G. Louie, *Phys. Rev. Lett.*, 2006, **97**, 216405.
52 K. S. Thygesen and A. Rubio, *Phys. Rev. Lett.*, 2009, **102**, 046802.
53 P. Umari, L. Giacomazzi, F. D. Angelis, M. Pastore and S. Baroni, *J. Chem. Phys.*, 2013, **139**, 014709.
54 M. Govoni and G. Galli, *J. Chem. Theory Comput.*, 2015, **11**, 2680–2696.
55 E. E. Salpeter and H. A. Bethe, *Phys. Rev.*, 1951, **84**, 1232–1242.
56 C. Kittel, *Introduction to Solid-State Physics*, John Wiley and Sons, 8th edn, 2004.
57 R. J. Elliott, *Phys. Rev.*, 1957, **108**, 1384–1389.
58 W. Hanke and L. J. Sham, *Phys. Rev. Lett.*, 1979, **43**, 387–390.
59 G. Onida, L. Reining, R. W. Godby, R. Del Sole and W. Andreoni, *Phys. Rev. Lett.*, 1995, **75**, 818–821.
60 M. Rohlfing and S. G. Louie, *Phys. Rev. Lett.*, 1998, **80**, 3320–3323.
61 S. Albrecht, L. Reining, R. Del Sole and G. Onida, *Phys. Rev. Lett.*, 1998, **80**, 4510–4513.
62 M. Rohlfing and S. G. Louie, *Phys. Rev. Lett.*, 1998, **81**, 2312–2315.
63 L. X. Benedict, E. L. Shirley and R. B. Bohn, *Phys. Rev. Lett.*, 1998, **80**, 4514–4517.
64 M. Rohlfing and S. G. Louie, *Phys. Rev. Lett.*, 1999, **82**, 1959–1962.
65 J.-W. van der Horst, P. A. Bobbert, M. A. J. Michels, G. Brocks and P. J. Kelly, *Phys. Rev. Lett.*, 1999, **83**, 4413–4416.
66 J.-W. van der Horst, P. A. Bobbert, P. H. L. de Jong, M. A. J. Michels, G. Brocks and P. J. Kelly, *Phys. Rev. B: Condens. Matter Mater. Phys.*, 2000, **61**, 15817–15826.
67 J. van der Horst, P. Bobbert, M. Michels and H. Bässler, *J. Chem. Phys.*, 2001, **114**, 6950–6957.
68 P. Puschnig and C. Ambrosch-Draxl, *Phys. Rev. Lett.*, 2002, **89**, 056405.
69 M. L. Tiago, M. Rohlfing and S. G. Louie, *Phys. Rev. B: Condens. Matter Mater. Phys.*, 2004, **70**, 193204.
70 M. L. Tiago, J. E. Northrup and S. G. Louie, *Phys. Rev. B: Condens. Matter Mater. Phys.*, 2003, **67**, 115212.
71 K. Hummer, P. Puschnig and C. Ambrosch-Draxl, *Phys. Rev. Lett.*, 2004, **92**, 147402.
72 K. Hummer and C. Ambrosch-Draxl, *Phys. Rev. B: Condens. Matter Mater. Phys.*, 2005, **71**, 081202.
73 N. Sai, M. L. Tiago, J. R. Chelikowsky and F. A. Reboredo, *Phys. Rev. B: Condens. Matter Mater. Phys.*, 2008, **77**, 161306.
74 C. Ambrosch-Draxl, D. Nabok, P. Puschnig and C. Meisenbichler, *New J. Phys.*, 2009, **11**, 125010.
75 P. Cudazzo, M. Gatti and A. Rubio, *Phys. Rev. B: Condens. Matter Mater. Phys.*, 2012, **86**, 195307.
76 S. Sharifzadeh, A. Biller, L. Kronik and J. B. Neaton, *Phys. Rev. B: Condens. Matter Mater. Phys.*, 2012, **85**, 125307.
77 S. Sharifzadeh, P. Darancet, L. Kronik and J. B. Neaton, *J. Phys. Chem. Lett.*, 2013, **4**, 2197–2201.
78 P. Cudazzo, M. Gatti, A. Rubio and F. Sottile, *Phys. Rev. B: Condens. Matter Mater. Phys.*, 2013, **88**, 195152.
79 C. Cocchi and C. Draxl, *Phys. Rev. B: Condens. Matter Mater. Phys.*, 2015, **92**, 205126.
80 C. Cocchi and C. Draxl, *Phys. Rev. B: Condens. Matter Mater. Phys.*, 2015, **92**, 205105.
81 P. Cudazzo, F. Sottile, A. Rubio and M. Gatti, *J. Phys.: Condens. Matter*, 2015, **27**, 113204.
82 X. Leng, H. Yin, D. Liang and Y. Ma, *J. Chem. Phys.*, 2015, **143**, 114501.
83 T. Rangel, K. Berland, S. Sharifzadeh, F. Brown-Altvater, K. Lee, P. Hyldgaard, L. Kronik and J. B. Neaton, *Phys. Rev. B: Condens. Matter Mater. Phys.*, 2016, **93**, 115206.
84 X. Leng, J. Feng, T. Chen, C. Liu and Y. Ma, *Phys. Chem. Chem. Phys.*, 2016, **18**, 30777–30784.
85 X. Wang, T. Garcia, S. Monaco, B. Schatschneider and N. Marom, *CrystEngComm*, 2016, **18**, 7353–7362.
86 J. C. Grossman, M. Rohlfing, L. Mitas, S. G. Louie and M. L. Cohen, *Phys. Rev. Lett.*, 2001, **86**, 472–475.
87 M. L. Tiago and J. Chelikowsky, *Solid State Commun.*, 2005, **136**, 333–337.
88 M. L. Tiago, P. R. C. Kent, R. Q. Hood and F. A. Reboredo, *J. Chem. Phys.*, 2008, **129**, 084311.
89 M. Palummo, C. Hogan, F. Sottile, P. Bagalá and A. Rubio, *J. Chem. Phys.*, 2009, **131**, 084102.
90 Y. Ma, M. Rohlfing and C. Molteni, *Phys. Rev. B: Condens. Matter Mater. Phys.*, 2009, **80**, 241405.
91 Y. Ma, M. Rohlfing and C. Molteni, *J. Chem. Theory Comput.*, 2010, **6**, 257–265.
92 M. S. Kaczmarski, Y. Ma and M. Rohlfing, *Phys. Rev. B: Condens. Matter Mater. Phys.*, 2010, **81**, 115433.
93 D. Rocca, D. Lu and G. Galli, *J. Chem. Phys.*, 2010, **133**, 164109.
94 J. M. Garcia-Lastra and K. S. Thygesen, *Phys. Rev. Lett.*, 2011, **106**, 187402.
95 X. Blase and C. Attaccalite, *Appl. Phys. Lett.*, 2011, **99**, 171909.
96 I. Duchemin, T. Deutsch and X. Blase, *Phys. Rev. Lett.*, 2012, **109**, 167801.
97 B. Baumeier, D. Andrienko, Y. Ma and M. Rohlfing, *J. Chem. Theory Comput.*, 2012, **8**, 997–1002.
98 B. Baumeier, D. Andrienko and M. Rohlfing, *J. Chem. Theory Comput.*, 2012, **8**, 2790–2795.
99 C. Faber, P. Boulanger, I. Duchemin, C. Attaccalite and X. Blase, *J. Chem. Phys.*, 2013, **139**, 194308.
100 I. Duchemin and X. Blase, *Phys. Rev. B: Condens. Matter Mater. Phys.*, 2013, **87**, 245412.
101 B. Baumeier, M. Rohlfing and D. Andrienko, *J. Chem. Theory Comput.*, 2014, **10**, 3104–3110.
102 D. Varsano, E. Coccia, O. Pulci, A. M. Conte and L. Guidoni, *Comput. Theor. Chem.*, 2014, **1040**, 338–346.
103 E. Coccia, D. Varsano and L. Guidoni, *J. Chem. Theory Comput.*, 2014, **10**, 501–506.
104 P. Boulanger, S. Chibani, B. Le Guennic, I. Duchemin, X. Blase and D. Jacquemin, *J. Chem. Theory Comput.*, 2014, **10**, 4548–4556.

105 P. Boulanger, D. Jacquemin, I. Duchemin and X. Blase, *J. Chem. Theory Comput.*, 2014, **10**, 1212–1218.
106 Y. Noguchi, M. Hiyama, H. Akiyama and N. Koga, *J. Chem. Phys.*, 2014, **141**, 044309.
107 H. Yin, Y. Ma, J. Mu, C. Liu and M. Rohlfing, *Phys. Rev. Lett.*, 2014, **112**, 228301.
108 S. Körbel, P. Boulanger, I. Duchemin, X. Blase, M. A. L. Marques and S. Botti, *J. Chem. Theory Comput.*, 2014, **10**, 3934–3943.
109 D. Hirose, Y. Noguchi and O. Sugino, *Phys. Rev. B: Condens. Matter Mater. Phys.*, 2015, **91**, 205111.
110 M. P. Ljungberg, P. Koval, F. Ferrari, D. Foerster and D. Sánchez-Portal, *Phys. Rev. B: Condens. Matter Mater. Phys.*, 2015, **92**, 075422.
111 R. Cardia, G. Malloci, G.-M. Rignanese, X. Blase, E. Molteni and G. Cappellini, *Phys. Rev. B: Condens. Matter Mater. Phys.*, 2016, **93**, 235132.
112 F. Gala, L. Mattiello, F. Brunetti and G. Zollo, *J. Chem. Phys.*, 2016, **144**, 084310.
113 X. Blase, P. Boulanger, F. Bruneval, M. Fernandez-Serra and I. Duchemin, *J. Chem. Phys.*, 2016, **144**, 034109.
114 V. Ziaei and T. Bredow, *J. Chem. Phys.*, 2016, **145**, 174305.
115 M. Marsili, E. Mosconi, F. De Angelis and P. Umari, *Phys. Rev. B*, 2017, **95**, 075415.
116 K. Krause and W. Klopper, *J. Comput. Chem.*, 2017, **38**, 383–388.
117 J. Wehner and B. Baumeier, *J. Chem. Theory Comput.*, 2017, **13**, 1584–1594.
118 D. Hirose, Y. Noguchi and O. Sugino, *J. Chem. Phys.*, 2017, **146**, 044303.
119 L. Hung, F. Bruneval, K. Baishya and S. Öğüt, *J. Chem. Theory Comput.*, 2017, **13**, 2135–2146.
120 Y. Noguchi and O. Sugino, *J. Chem. Phys.*, 2017, **146**, 144304.
121 V. Ziaei and T. Bredow, *ChemPhysChem*, 2017, **18**, 579–583.
122 D. Escudero, I. Duchemin, X. Blase and D. Jacquemin, *J. Phys. Chem. Lett.*, 2017, **8**, 936–940.
123 D. Jacquemin, I. Duchemin and X. Blase, *J. Chem. Theory Comput.*, 2015, **11**, 3290–3304.
124 F. Bruneval, S. M. Hamed and J. B. Neaton, *J. Chem. Phys.*, 2015, **142**, 244101.
125 D. Jacquemin, I. Duchemin and X. Blase, *J. Chem. Theory Comput.*, 2015, **11**, 5340–5359.
126 D. Jacquemin, I. Duchemin, A. Blondel and X. Blase, *J. Chem. Theory Comput.*, 2016, **12**, 3969–3981.
127 C. Azarias, I. Duchemin, X. Blase and D. Jacquemin, *J. Chem. Phys.*, 2017, **146**, 034301.
128 D. Jacquemin, I. Duchemin, A. Blondel and X. Blase, *J. Chem. Theory Comput.*, 2017, **13**, 767–783.
129 T. Rangel, S. M. Hamed, F. Bruneval and J. B. Neaton, *J. Chem. Phys.*, 2017, **146**, 194108.
130 C. Azarias, C. Habert, Š. Budzák, X. Blase, I. Duchemin and D. Jacquemin, *J. Phys. Chem. A*, 2017, **121**, 6122–6134.
131 D. Jacquemin, I. Duchemin and X. Blase, *J. Phys. Chem. Lett.*, 2017, **8**, 1524–1529.
132 C. Holzer and W. Klopper, *J. Chem. Phys.*, 2017, **147**, 181101.
133 A. M. Conte, L. Guidoni, R. D. Sole and O. Pulci, *Chem. Phys. Lett.*, 2011, **515**, 290–295.
134 E. Coccia, D. Varsano and L. Guidoni, *J. Chem. Theory Comput.*, 2017, **13**, 4357–4367.
135 D. Varsano, S. Caprasecca and E. Coccia, *J. Phys.: Condens. Matter*, 2017, **29**, 013002.
136 D. Niedzialek, I. Duchemin, T. B. de Queiroz, S. Osella, A. Rao, R. Friend, X. Blase, S. Kümmel and D. Beljonne, *Adv. Funct. Mater.*, 2015, **25**, 1972–1984.
137 T. Hahn, J. Geiger, X. Blase, I. Duchemin, D. Niedzialek, S. Tscheuschner, D. Beljonne, H. Bässler and A. Köhler, *Adv. Funct. Mater.*, 2015, **25**, 1287–1295.
138 C. Faber, I. Duchemin, T. Deutsch and X. Blase, *Phys. Rev. B: Condens. Matter Mater. Phys.*, 2012, **86**, 155315.
139 N. Dardenne, R. Cardia, J. Li, G. Malloci, G. Cappellini, X. Blase, J.-C. Charlier and G.-M. Rignanese, *J. Phys. Chem. C*, 2017, **121**, 24480–24488.
140 T. Rangel, S. M. Hamed, F. Bruneval and J. B. Neaton, *J. Chem. Theory Comput.*, 2016, **12**, 2834–2842.
141 C. Hogan, M. Palummo, J. Gierschner and A. Rubio, *J. Chem. Phys.*, 2013, **138**, 024312.
142 B. Bagheri, M. Karttunen and B. Baumeier, *Eur. Phys. J.: Spec. Top.*, 2016, **225**, 1743–1756.
143 P. H. Hahn, W. G. Schmidt, K. Seino, M. Preuss, F. Bechstedt and J. Bernholc, *Phys. Rev. Lett.*, 2005, **94**, 037404.
144 V. Garbuio, M. Cascella, L. Reining, R. D. Sole and O. Pulci, *Phys. Rev. Lett.*, 2006, **97**, 137402.
145 A. Hermann, W. G. Schmidt and P. Schwerdtfeger, *Phys. Rev. Lett.*, 2008, **100**, 207403.
146 A. Hermann and P. Schwerdtfeger, *Phys. Rev. Lett.*, 2011, **106**, 187403.
147 M. Rohrmüller, S. Herres-Pawlis, M. Witte and W. G. Schmidt, *J. Comput. Chem.*, 2013, **34**, 1035–1045.
148 A. Jesser, M. Rohrmüller, W. G. Schmidt and S. Herres-Pawlis, *J. Comput. Chem.*, 2014, **35**, 1–17.
149 A. Hoffmann, M. Rohrmüller, A. Jesser, I. dos Santos Vieira, W. G. Schmidt and S. Herres-Pawlis, *J. Comput. Chem.*, 2014, **35**, 2146–2161.
150 S. Kümmel and L. Kronik, *Rev. Mod. Phys.*, 2008, **80**, 3–60.
151 A. D. Becke, *J. Chem. Phys.*, 1993, **98**, 5648–5652.
152 A. D. Becke, *J. Chem. Phys.*, 1993, **98**, 1372–1377.
153 C. Adamo and V. Barone, *J. Chem. Phys.*, 1999, **110**, 6158–6170.
154 T. Yanai, D. P. Tew and N. C. Handy, *Chem. Phys. Lett.*, 2004, **393**, 51–56.
155 O. A. Vydrov and G. E. Scuseria, *J. Chem. Phys.*, 2006, **125**, 234109.
156 Y. Zhao and D. G. Truhlar, *Acc. Chem. Res.*, 2008, **41**, 157–167.
157 S. Refaely-Abramson, R. Baer and L. Kronik, *Phys. Rev. B: Condens. Matter Mater. Phys.*, 2011, **84**, 075144.
158 T. Körzdörfer and J.-L. Brédas, *Acc. Chem. Res.*, 2014, **47**, 3284–3291.
159 L. Gallandi, N. Marom, P. Rinke and T. Körzdörfer, *J. Chem. Theory Comput.*, 2016, **12**, 605–614.
160 G. Stefanucci and R. van Leeuwen, *Nonequilibrium Many-Body Theory of Quantum Systems: A Modern Introduction*, Cambridge University Press, Cambridge, UK, 2013.

161 T. Körzdörfer and N. Marom, *Phys. Rev. B: Condens. Matter Mater. Phys.*, 2012, **86**, 041110.
162 F. Bruneval and M. A. L. Marques, *J. Chem. Theory Comput.*, 2013, **9**, 324–329.
163 J. W. Knight, X. Wang, L. Gallandi, O. Dolgounitcheva, X. Ren, J. V. Ortiz, P. Rinke, T. Körzdörfer and N. Marom, *J. Chem. Theory Comput.*, 2016, **12**, 615–626.
164 M. van Schilfgaarde, T. Kotani and S. Faleev, *Phys. Rev. Lett.*, 2006, **96**, 226402.
165 C. Faber, C. Attaccalite, V. Olevano, E. Runge and X. Blase, *Phys. Rev. B: Condens. Matter Mater. Phys.*, 2011, **83**, 115123.
166 P. Koval, D. Foerster and D. Sánchez-Portal, *Phys. Rev. B: Condens. Matter Mater. Phys.*, 2014, **89**, 155417.
167 K. Krause, M. E. Harding and W. Klopper, *Mol. Phys.*, 2015, **113**, 1952–1960.
168 F. Kaplan, M. E. Harding, C. Seiler, F. Weigend, F. Evers and M. J. van Setten, *J. Chem. Theory Comput.*, 2016, **12**, 2528–2541.
169 Y. M. Rhee and M. Head-Gordon, *J. Phys. Chem. A*, 2007, **111**, 5314–5326.
170 H. N. Rojas, R. W. Godby and R. J. Needs, *Phys. Rev. Lett.*, 1995, **74**, 1827–1830.
171 D. Neuhauser, Y. Gao, C. Arntsen, C. Karshenas, E. Rabani and R. Baer, *Phys. Rev. Lett.*, 2014, **113**, 076402.
172 P. Liu, M. Kaltak, J. C. V. Klimeš and G. Kresse, *Phys. Rev. B: Condens. Matter Mater. Phys.*, 2016, **94**, 165109.
173 D. Roca-Sanjuán, M. Rubio, M. Merchán and L. Serrano-Andrés, *J. Chem. Phys.*, 2006, **125**, 084302.
174 M. R. Silva-Junior, M. Schreiber, S. P. A. Sauer and W. Thiel, *J. Chem. Phys.*, 2010, **133**, 174318.
175 M. Schreiber, M. R. Silva-Junior, S. P. A. Sauer and W. Thiel, *J. Chem. Phys.*, 2008, **128**, 134110.
176 M. R. Silva-Junior, S. P. A. Sauer, M. Schreiber and W. Thiel, *Mol. Phys.*, 2010, **108**, 453–465.
177 D. Jacquemin, V. Wathelet, E. A. Perpète and C. Adamo, *J. Chem. Theory Comput.*, 2009, **5**, 2420–2435.
178 C. E. Hoyer, S. Ghosh, D. G. Truhlar and L. Gagliardi, *J. Phys. Chem. Lett.*, 2016, **7**, 586–591.
179 N. O. C. Winter, N. K. Graf, S. Leutwyler and C. Hattig, *Phys. Chem. Chem. Phys.*, 2013, **15**, 6623–6630.
180 D. Jacquemin, B. Moore, A. Planchat, C. Adamo and J. Autschbach, *J. Chem. Theory Comput.*, 2014, **10**, 1677–1685.
181 D. Jacquemin, I. Duchemin and X. Blase, *Mol. Phys.*, 2015, **114**, 957–967.
182 A. Laurent, A. Blondel and D. Jacquemin, *Theor. Chem. Acc.*, 2015, **134**, 76.
183 D. Jacquemin, A. Planchat, C. Adamo and B. Mennucci, *J. Chem. Theory Comput.*, 2012, **8**, 2359–2372.
184 T. Tawada, T. Tsuneda, S. Yanagisawa, T. Yanai and K. Hirao, *J. Chem. Phys.*, 2004, **120**, 8425–8433.
185 M. Miura, Y. Aoki and B. Champagne, *J. Chem. Phys.*, 2007, **127**, 084103.
186 M. R. Silva-Junior, M. Schreiber, S. P. A. Sauer and W. Thiel, *J. Chem. Phys.*, 2008, **129**, 104103.
187 M. Caricato, G. W. Trucks, M. J. Frisch and K. B. Wiberg, *J. Chem. Theory Comput.*, 2011, **7**, 456–466.
188 P. G. Szalay, T. Watson, A. Perera, V. F. Lotrich and R. J. Bartlett, *J. Phys. Chem. A*, 2012, **116**, 6702–6710.
189 P. H. P. Harbach, M. Wormit and A. Dreuw, *J. Chem. Phys.*, 2014, **141**, 064113.
190 D. Kánnár and P. G. Szalay, *J. Chem. Theory Comput.*, 2014, **10**, 3757–3765.
191 S. P. Sauer, H. F. Pitzner-Frydendahl, M. Buse, H. J. A. Jensen and W. Thiel, *Mol. Phys.*, 2015, **113**, 2026–2045.
192 D. J. Tozer, *J. Chem. Phys.*, 2003, **119**, 12697–12699.
193 A. Dreuw, J. L. Weisman and M. Head-Gordon, *J. Chem. Phys.*, 2003, **119**, 2943–2946.
194 A. Dreuw and M. Head-Gordon, *J. Am. Chem. Soc.*, 2004, **126**, 4007–4016.
195 R. J. Magyar and S. Tretiak, *J. Chem. Theory Comput.*, 2007, **3**, 976–987.
196 Z. L. Cai, M. J. Crossley, J. R. Reimers, R. Kobayashi and R. D. Amos, *J. Phys. Chem. B*, 2006, **110**, 15624–15632.
197 R. S. Mulliken, *J. Am. Chem. Soc.*, 1952, **74**, 811–824.
198 T. Stein, L. Kronik and R. Baer, *J. Am. Chem. Soc.*, 2009, **131**, 2818–2820.
199 R. Kobayashi and R. D. Amos, *Chem. Phys. Lett.*, 2006, **420**, 106–109.
200 M. J. G. Peach, P. Benfield, T. Helgaker and D. J. Tozer, *J. Chem. Phys.*, 2008, **128**, 044118.
201 T. Le Bahers, C. Adamo and I. Ciofini, *J. Chem. Theory Comput.*, 2011, **8**, 2498–2506.
202 C. A. Guido, P. Cortona, B. Mennucci and C. Adamo, *J. Chem. Theory Comput.*, 2013, **9**, 3118–3126.
203 F. Plasser, B. Thomitzni, S. A. Bäppler, J. Wenzel, D. R. Rehn, M. Wormit and A. Dreuw, *J. Comput. Chem.*, 2015, **36**, 1609–1620.
204 L. Reining, V. Olevano, A. Rubio and G. Onida, *Phys. Rev. Lett.*, 2002, **88**, 066404.
205 S. Botti, F. Sottile, N. Vast, V. Olevano, L. Reining, H.-C. Weissker, A. Rubio, G. Onida, R. Del Sole and R. W. Godby, *Phys. Rev. B: Condens. Matter Mater. Phys.*, 2004, **69**, 155112.
206 G. Ulrich, R. Ziessel and A. Harriman, *Angew. Chem., Int. Ed.*, 2008, **47**, 1184–1201.
207 M. Schreiber, V. Bub and M. P. Fülscher, *Phys. Chem. Chem. Phys.*, 2001, **3**, 3906–3912.
208 D. Jacquemin, E. A. Perpète, G. Scalmani, M. J. Frisch, R. Kobayashi and C. Adamo, *J. Chem. Phys.*, 2007, **126**, 144105.
209 R. Send, O. Valsson and C. Filippi, *J. Chem. Theory Comput.*, 2011, **7**, 444–455.
210 H. Zhekova, M. Krykunov, J. Autschbach and T. Ziegler, *J. Chem. Theory Comput.*, 2014, **10**, 3299–3307.
211 M. Filatov and M. Huix-Rotllant, *J. Chem. Phys.*, 2014, **141**, 024112.
212 S. Grimme and F. Neese, *J. Chem. Phys.*, 2007, **127**, 154116.
213 S. Hirata and M. Head-Gordon, *Chem. Phys. Lett.*, 1999, **314**, 291–299.
214 M. E. Casida, F. Gutierrez, J. Guan, F.-X. Gadea, D. Salahub and J.-P. Daudey, *J. Chem. Phys.*, 2000, **113**, 7062–7071.
215 J. S. Sears, T. Körzdörfer, C.-R. Zhang and J.-L. Brédas, *J. Chem. Phys.*, 2011, **135**, 151103.

216 D. Varsano, S. Caprasecca and E. Coccia, *J. Phys.: Condens. Matter*, 2016, **29**, 013002.
217 S. Refaely-Abramson, F. H. da Jornada, S. G. Louie and J. B. Neaton, 2011, arXiv:1706.01564.
218 C. Poelking, M. Tietze, C. Elschner, S. Olthof, D. Hertel, B. Baumeier, F. Würthner, K. Meerholz, K. Leo and D. Andrienko1, *Nat. Mater.*, 2015, **14**, 434.
219 J. Tomasi, B. Mennucci and R. Cammi, *Chem. Rev.*, 2005, **105**, 2999–3094.
220 N. Murugan, J. Kongsted, Z. Rinkevicius and H. Ågren, *Phys. Chem. Chem. Phys.*, 2011, **14**, 1107–1112.
221 A. Monari, J.-L. Rivail and X. Assfeld, *Acc. Chem. Res.*, 2013, **46**, 596–603.
222 K. Aidas, J. M. H. Olsen, J. Kongsted and H. Ågren, *J. Phys. Chem. B*, 2013, **117**, 2069–2080.
223 M. Rohlfing, *Phys. Rev. B: Condens. Matter Mater. Phys.*, 2010, **82**, 205127.
224 I. Tamblyn, P. Darancet, S. Y. Quek, S. A. Bonev and J. B. Neaton, *Phys. Rev. B: Condens. Matter Mater. Phys.*, 2011, **84**, 201402.
225 T. Rangel, A. Ferretti, P. E. Trevisanutto, V. Olevano and G.-M. Rignanese, *Phys. Rev. B: Condens. Matter Mater. Phys.*, 2011, **84**, 045426.
226 M. Rohlfing, *Phys. Rev. Lett.*, 2012, **108**, 087402.
227 K. T. Winther and K. S. Thygesen, *2D Mater.*, 2017, **4**, 025059.
228 I. Duchemin, D. Jacquemin and X. Blase, *J. Chem. Phys.*, 2016, **144**, 164106.
229 For a full quantum mechanical BSE/GW description of solvated nucleobasis, see ref. 107.
230 J. Li, G. D'Avino, I. Duchemin, D. Beljonne and X. Blase, *J. Phys. Chem. Lett.*, 2016, **7**, 2814–2820.
231 J. Li, G. D'Avino, A. Pershin, D. Jacquemin, I. Duchemin, D. Beljonne and X. Blase, *Phys. Rev. Mater.*, 2017, **1**, 025602.
232 A. Sitt, L. Kronik, S. Ismail-Beigi and J. R. Chelikowsky, *Phys. Rev. A: At., Mol., Opt. Phys.*, 2007, **76**, 054501.
233 J. Liu and W. Liang, *J. Chem. Phys.*, 2011, **135**, 014113.
234 T. Tsukagoshi and O. Sugino, *Phys. Rev. A: At., Mol., Opt. Phys.*, 2012, **86**, 064501.
235 J. A. Bjorgaard, K. A. Velizhanin and S. Tretiak, *J. Chem. Phys.*, 2015, **143**, 054305.
236 C. A. Guido, G. Scalmani, B. Mennucci and D. Jacquemin, *J. Chem. Phys.*, 2017, **146**, 204106.
237 C. Faber, J. L. Janssen, M. Côté, E. Runge and X. Blase, *Phys. Rev. B: Condens. Matter Mater. Phys.*, 2011, **84**, 155104.
238 C. Faber, P. Boulanger, C. Attaccalite, E. Cannuccia, I. Duchemin, T. Deutsch and X. Blase, *Phys. Rev. B: Condens. Matter Mater. Phys.*, 2015, **91**, 155109.
239 B. Ramberger, T. Schäfer and G. Kresse, *Phys. Rev. Lett.*, 2017, **118**, 106403.
240 G. Vignale and W. Kohn, *Phys. Rev. Lett.*, 1996, **77**, 2037–2040.
241 M. E. Casida, *J. Chem. Phys.*, 2005, **122**, 054111.
242 N. T. Maitra, F. Zhang, R. J. Cave and K. Burke, *J. Chem. Phys.*, 2004, **120**, 5932–5937.
243 P. Romaniello, D. Sangalli, J. A. Berger, F. Sottile, L. G. Molinari, L. Reining and G. Onida, *J. Chem. Phys.*, 2009, **130**, 044108.
244 D. Sangalli, P. Romaniello, G. Onida and A. Marini, *J. Chem. Phys.*, 2011, **134**, 034115.
245 D. Zhang, S. N. Steinmann and W. Yang, *J. Chem. Phys.*, 2013, **139**, 154109.
246 E. Rebolini and J. Toulouse, *J. Chem. Phys.*, 2016, **144**, 094107.
247 A. Schindlmayr and R. W. Godby, *Phys. Rev. Lett.*, 1998, **80**, 1702–1705.
248 L. Hung, F. H. da Jornada, J. Souto-Casares, J. R. Chelikowsky, S. G. Louie and S. Ögüt, *Phys. Rev. B: Condens. Matter Mater. Phys.*, 2016, **94**, 085125.
249 E. Maggio and G. Kresse, *J. Chem. Theory Comput.*, 2017, **13**, 4765–4778.
250 M. Shishkin, M. Marsman and G. Kresse, *Phys. Rev. Lett.*, 2007, **99**, 246403.
251 J. Wilhelm and J. Hutter, *Phys. Rev. B*, 2017, **95**, 235123.
252 M. Rohlfing, P. Krüger and J. Pollmann, *Phys. Rev. B: Condens. Matter Mater. Phys.*, 1993, **48**, 17791–17805.
253 D. Foerster, P. Koval and D. Sánchez-Portal, *J. Chem. Phys.*, 2011, **135**, 074105.